Journal of the Endocrine Society, 2023, **7**, 1–20
https://doi.org/10.1210/jendso/bvad095
Advance access publication 24 July 2023
Research Article

Grape Polyphenols May Prevent High-Fat Diet–Induced Dampening of the Hypothalamic–Pituitary–Adrenal Axis in Male Mice

Esther Mezhibovsky,[1,2] Kevin M. Tveter,[1] Jose A. Villa-Rodriguez,[1] Karen Bacalia,[1,2] Dushyant Kshatriya,[2,3] Nikhil Desai,[1] Alrick Cabales,[1] Yue Wu,[1] Ke Sui,[1] Rocio M. Duran,[1] Nicholas T. Bello,[3] and Diana E. Roopchand[1,2]

[1]Department of Food Science and NJ Institute for Food Nutrition and Health (Rutgers Center for Lipid Research; Center for Nutrition Microbiome and Health), Rutgers, The State University of New Jersey, New Brunswick, NJ 08901, USA
[2]Department of Nutritional Sciences Graduate Program, Rutgers, The State University of New Jersey, New Brunswick, NJ 08901, USA
[3]Department of Animal Sciences, Rutgers, The State University of New Jersey, New Brunswick, NJ 08901, USA

Correspondence: Diana E. Roopchand, PhD, Department of Food Science and NJ Institute for Food Nutrition and Health (Rutgers Center for Lipid Research; Center for Nutrition Microbiome and Health), Rutgers, The State University of New Jersey, 61 Dudley Road, New Brunswick, NJ 08901, USA. Email: roopchand@sebs.rutgers.edu.

Abstract

Context : Chronic high-fat diet (HFD) consumption causes obesity associated with retention of bile acids (BAs) that suppress important regulatory axes, such as the hypothalamic–pituitary–adrenal axis (HPAA). HFD impairs nutrient sensing and energy balance due to a dampening of the HPAA and reduced production and peripheral metabolism of corticosterone (CORT).

Objective: We assessed whether proanthocyanidin-rich grape polyphenol (GP) extract can prevent HFD-induced energy imbalance and HPAA dysregulation.

Methods: Male C57BL6/J mice were fed HFD or HFD supplemented with 0.5% w/w GPs (HFD-GP) for 17 weeks.

Results: GP supplementation reduced body weight gain and liver fat while increasing circadian rhythms of energy expenditure and HPAA-regulating hormones, CORT, leptin, and PYY. GP-induced improvements were accompanied by reduced mRNA levels of *Il6*, *Il1b*, and *Tnfa* in ileal or hepatic tissues and lower cecal abundance of Firmicutes, including known BA metabolizers. GP-supplemented mice had lower concentrations of circulating BAs, including hydrophobic and HPAA-inhibiting BAs, but higher cecal levels of taurine-conjugated BAs antagonistic to farnesoid X receptor (FXR). Compared with HFD-fed mice, GP-supplemented mice had increased mRNA levels of hepatic *Cyp7a1* and *Cyp27a1*, suggesting reduced FXR activation and more BA synthesis. GP-supplemented mice also had reduced hepatic *Abcc3* and ileal *Ibabp* and *Ostβ*, indicative of less BA transfer into enterocytes and circulation. Relative to HFD-fed mice, CORT and BA metabolizing enzymes (*Akr1d1* and *Srd5a1*) were increased, and *Hsd11b1* was decreased in GP supplemented mice.

Conclusion: GPs may attenuate HFD-induced weight gain by improving hormonal control of the HPAA and inducing a BA profile with less cytotoxicity and HPAA inhibition, but greater FXR antagonism.

Key Words: proanthocyanidins, high-fat diet, bile acids, gut microbiota, diet induced obesity, hypothalamic–pituitary–adrenal axis, corticosterone, farnesoid X receptor, leptin, peptide YY

Abbreviations: 5α-DH-CORT, 5α-dihydrocorticosterone; 5α-TH-CORT, 5α-tetrahydrocorticosterone; 11β-HSD1, 11-beta-hydroxysteroid dehydrogenase; 11-DH-CORT, 11-dehydrocorticosterone; αMCA, alpha-muricholic acid; βMCA, beta-muricholic acid; ωMCA, omega-muricholic acid; AKR1D1, aldo-keto-reductase family 1 member D1; ANOVA, analysis of variance; AP, area postrema; ASV, amplicon sequence variant; BA, bile acid; CA, cholic acid; CDCA, chenodeoxycholic acid; CV, calorific value; CYP7A1, cytochrome P450 family 7 subfamily A member 1; CYP27A1, cytochrome P450 family 27 subfamily A member 1; CORT, corticosterone; CRH, corticotropin-releasing hormone; DCA, deoxycholic acid; FXR, farnesoid X receptor; GCA, glycocholic acid; GCDCA, glycochenodeoxycholic acid; GDCA, glycodeoxycholic acid; GHCA, glycohyocholic acid; GLCA, glycolithocholic acid; GUDCA, glycoursodeoxycholic acid; GP, grape polyphenol; HCA, hyocholic acid; HDCA, hyodeoxycholic acid; HFD, high-fat diet; HPG, hypothalamic pituitary gonadal; HPAA, hypothalamic–pituitary–adrenal axis; HPLC, high-performance liquid chromatography; IL, interleukin; IS, internal standard; LCMS, liquid chromatography mass spectrometry; LFD, low fat diet; MS, mass spectrometer; NCA, nutracholic acid; NTS, nucleus of the solitary tract; OATP, organic anion transport protein; PBA, primary bile acid; PBS, phosphate-buffered saline; PYY, peptide YY; RER, respiratory exchange ratio; SBA, secondary bile acid; SCFA, short chain fatty acid; SPI, soy protein isolate; SRD5A1, steroid 5 alpha-reductase 1; TαMCA, tauro-alpha-muricholic acid; TβMCA, tauro-beta-muricholic acid; TωMCA, tauro-omega-muricholic acid; TBA, total bile acid; TCA, taurocholic acid; TCDCA, taurochenodeoxycholic acid; TDCA, taurodeoxycholic acid; THDCA, taurohyodeoxycholic acid; TLCA, taurolithocholic acid; TNF, tumor necrosis factor; TUDCA, tauroursodeoxycholic acid; UDCA, ursodeoxycholic acid.

Excessive fat and sugar intake leads to obesity and associated comorbidities [1, 2]. Understanding how dietary polyphenols improve metabolic health can inform recommendations for nutrition, supplements, and drug development. Grape polyphenols (GPs) rich in B-type proanthocyanidins were found to attenuate diet-induced body weight gain, gut dysbiosis,

Received: 8 March 2023. **Editorial Decision:** 14 July 2023. **Corrected and Typeset:** 2 August 2023

fatty liver, glucose intolerance, and inflammation in male C57BL/6 mice [3-6]. These metabolic improvements were linked to increased energy expenditure, improved enteroendocrine sensitivity, altered bile acid (BA) and short chain fatty acid (SCFA) composition, and favorable gut microbial profiles [3-9].

The hypothalamic–pituitary–adrenal axis (HPAA) plays a central role in energy balance and is influenced by enteroendocrine hormones and steroid hormones such as BAs and glucocorticoids [10-12]. GP-induced metabolic improvements may involve modulations to the HPAA and its regulatory hormones. The HPAA coordinates energy resource allocations among organs (eg, liver, fat, intestine) based on factors such as waking vs sleeping hours, feeding, physical activity, injury, and disease [13, 14]. The HPAA operates in a circadian manner, with peak activity during daylight in humans and nighttime in rodents [15]. Upon stimulation, the paraventricular nucleus of the hypothalamus releases corticotropin-releasing hormone (CRH), which triggers release of adrenocorticotropic hormone from the pituitary gland, leading to the release of glucocorticosteroids from the adrenal glands [15]. Cortisol is the primary glucocorticoid in most mammals; however, rodents lack 17α-hydroxylase in the adrenal cortex to produce sufficient amounts of cortisol; as such, corticosterone (CORT) is regarded as the physiological marker of HPAA function in rodents [16]. Feedback regulation of the HPAA involves CORT [15], as well as peripheral hormones like leptin and peptide YY (PYY), produced by adipocytes and enterocytes, respectively [10, 11]. CORT levels are also regulated within the adrenal glands, liver, brain, and adipose by enzymes responsible for its deactivation (11β-HSD2), activation (11β-HSD1), or clearance (5α- and 5β-reductase) [17]. 11β-HSD1 and 5α- and 5β-reductases are also important for BA homeostasis as they convert cytotoxic BA intermediates to BA species important for emulsifying fats [18].

The metabolic stress imposed by chronic HFD intake impairs regulation of the HPAA and BA homeostasis via several mechanisms. Both BA metabolism and the HPAA are influenced by the circadian clock system which is uncoupled by HFD feeding [19-21]. Initially, the body responds to HFD by increasing CRH, CORT, and leptin production to increase energy expenditure and counteract weight gain [22-24]. However, prolonged HFD consumption leads to chronically elevated CORT levels, densitized feedback mechanisms, and eventual adrenal exhaustion, insufficiency, and finally reduced CORT levels and energy imbalance [12, 25, 10, 17, 21, 26]. Leptin-resistance [10] and reduced PYY levels [27] from chronic HFD feeding further dysregulates the HPAA. HFD also elevates BA concentrations, which can be toxic to both host and gut bacteria [28]. BAs may spillover from liver to circulation and increased blood brain barrier permeability to BAs that suppress the HPAA [12, 29-31]. Increased BA levels further hinder HPAA homeostasis by saturating the enzymes in peripheral organs responsible for CORT clearance [12]. To investigate whether GP supplementation protects against HFD-induced HPAA disruption, markers of HPAA activity, BA metabolism, and levels of BAs and SCFAs were measured.

Materials and Methods

GP Extract and Characterization

As previously described [4], GPs were extracted from frozen grape pomace (kindly provided by Welch Foods Inc., Concord, MA, USA). Colorimetric assays were used to measure total polyphenols using the Folin Ciocalteu assay using gallic acid as standard [32], and B-type proanthocyanidin levels using the 4-dimethylaminocinnamaldehyde assay [33] using B-type proanthocyanidins (Cayman Chemicals, catalog #19865) as standard. Dried GP extract comprised 14% (w/w) total polyphenols. To obtain a detailed biochemical profile, samples were also analyzed by a ultrahigh-pressure liquid chromatography mass spectrometry (UPLC/MS) system including the Dionex UltiMate 3000 RSLC UPLC system, consisting of a workstation with ThermoFisher Scientific's Xcalibur v. 4.0 software package combined with Dionex's SII LC control software, solvent rack/degasser SRD-3400, pulseless chromatography pump HPG-3400RS, autosampler WPS-3000RS, column compartment TCC-3000RS, and photodiode array detector DAD-3000RS. After the photodiode array detector the eluent flow was guided to a Q Exactive Plus Orbitrap high-resolution high-mass accuracy mass spectrometer (MS). Mass detection was full MS scan with low energy collision induced dissociation from 100 to 1000 *m/z* in negative ionization mode with electrospray interface. Sheath gas flow rate was 30 arbitrary units, auxiliary gas flow rate was 7, and sweep gas flow rate was 1. The spray voltage was −3500 V with a capillary temperature of 275 °C. The mass resolution was 70 000, or higher. Substances were separated on a Phenomenex Kinetex C8 reverse phase column, size 100 × 2 mm, particle size 2.6 mm, pore size 100 Å. The mobile phase consisted of 2 components: solvent A (0.5% ACS grade acetic acid in liquid chromatography mass spectrometry [LCMS] grade water, pH 3-3.5), and solvent B (100% acetonitrile, LCMS grade). The mobile phase flow was 0.20 mL/min, and a gradient mode was used for all analyses. The initial conditions of the gradient were 95% A and 5% B; for 30 minutes the proportion reaches 5% A and 95% B, which was kept for the next 8 minutes, and during the following 4 minutes the ratio was brought to initial conditions. An 8-minute equilibration interval was included between subsequent injections. The average pump pressure using these parameters was typically around 3900 psi for the initial conditions. Putative formulas of polyphenols were determined by performing isotope abundance analysis on the high-resolution mass spectral data with Xcalibur v. 4.0 software and reporting the best fitting empirical formula. Database searches were performed using www.reaxys.com (Elsevier Life Sciences IP Limited) and SciFinder (American Chemical Society). Polyphenol species, detected by UPLC/MS, in the GP extract used in this study, included a mixture of catechin/epicatechin monomers and proanthocyanidin B-type dimers, followed by trimers, dimer gallates, trimer gallates, tetramers, pentamers, as well as stilbenes and oligostilbenes (Fig. 1 [34]).

Diets

As previously described [4], GP extract was sorbed to soy protein isolate (SPI) to produce a GP–SPI complex standardized to deliver 5% GPs, of which approximately 72% were proanthocyanidins as determined by colorimetric assays. Nutritional analysis was performed on SPI and GP-SPI (Medallion Laboratories; Table 1 [34]) and this information was used to formulate ingredient-matched murine diets (Research Diets, NJ, USA): (1) low-fat diet (LFD), (2) HFD (62% kcal fat), and (3) HFD containing 10% w/w GP–SPI to deliver 0.5% w/w GPs (HFD-GP). HFD and HFD-GP were isocaloric (Table 2 [34]). LFD-fed

mice served as a control for HFD-induced obesity, fatty liver, and inflammation.

Animals

Five-week-old wild type male mice (C57BL/6J) purchased from Jackson Laboratory (Bar Harbor, ME, USA) were single-housed in ventilated cages with an igloo shelter. Data on stress (measured as urinary or serum CORT) associated with single verses group-housing is contradictory [35, 36]. Mice were initially group-housed to alleviate stress levels; however, due to fighting we observed significant differences in body weight, glucose tolerance, and hair loss among grouped animals, so mice were switched to a less stressful single-housing setting. Mice were placed on a 12-hour light/dark cycle (07:00 to 19:00 hours light) in a temperature-controlled room (24 °C ± 1 °C) with ad libitum access to food and water. Mice were fed LFD for a 2-week acclimation period then were randomized to receive LFD, HFD, or HFD-GP (n = 15/group) for 17 weeks. At the time of randomization, diet groups did not show baseline differences in body weights or glucose tolerance, as determined by an oral glucose tolerance test. Food intake, body weight, and body composition (EchoMRI 3-in-1 system; Echo Medical Systems, Houston, TX, USA) were measured as previously described [4]. After 17 weeks of the diet intervention, unfasted mice were euthanized by CO_2 asphyxiation (n = 9/group), after which cardiac blood was collected using 1-cc syringe and mice were decapitated. Mice were sacrificed over a span of 2 days. Cardiac blood (n = 7-9 mice/group) was collected into microfuge tubes and mixed with 50 μM dipeptidyl peptidase IV inhibitor (EMP Millipore, Billerica, MA, USA) and immediately stored on ice for 30 minutes. Serum was separated by centrifugation at 3000*g* for 25 minutes and stored at −80 °C until use. The largest liver lobe was used for all assays. Approximately 2.5 cm of the distal-most ileum was flushed with 1× phosphate-buffered saline (PBS) prior to storage. The entire hypothalamus was collected for gene expression analysis. Collected tissues were snap-frozen in liquid nitrogen and stored at 80 °C until use. A schematic of the study design including timepoints for the performed assays is elsewhere (Fig. 2 [34]).

Neural Activation Assay and c-Fos Immunolabeling

A subset of mice (n = 6/group) were used for neural activation assay to detect stimulation by glucose. Mice were given D-dextrose (2 g/kg) via oral gavage then were deeply anaesthetized with isoflurane/oxygen delivered by a nose cone, exsanguinated with 0.9% saline, and perfused with 4% paraformaldehyde in PBS. Brains were extracted and post-fixed for 24 hours in 4% paraformaldehyde in PBS, then switched to 20% sucrose in 4% paraformaldehyde until sectioning. Free-floating sections (40 μm) of the forebrain were obtained using a Leica cryostat (Leica Microsystems, Rijswijk, The Netherlands). Sections were stored in cryoprotectant until immunohistochemistry was performed. Sections were transferred to a new clean plate containing PBS (10 mM phosphate, 150 mM NaCl, pH 7.5). Initial PBS was removed; sections were then washed 3 × 10 minutes in PBS. Endogenous peroxidases were neutralized with 0.3% H_2O_2 in dH_2O. After a 3 × 10 minutes PBS wash, sections were incubated in normal goat serum (PK-4001, Vectastain ABC kit, Vector Laboratories, Burlingame, CA, USA) with 0.3% Triton-X-100 in PBS for 30 minutes. c-Fos immunolabeling was performed with a polyclonal rabbit IgG anti-c-Fos antibody (ab190289, Abcam, Cambridge, MA, USA; RRID: AB_2737414), diluted 1:100 in PBS. Tissue sections were incubated overnight (~20 hours). Sections were transferred to a new clean plate, washed 3 × 10 minutes in 0.1% Triton X-100 in PBS, then incubated for 30 minutes in biotinylated secondary antibody (goat IgG antirabbit, PK-4001, Vectastain ABC kit, Vector Laboratories, RRID:AB_2336810) with 0.3% Triton X-100 in PBS. After 3 × 10 minutes wash in PBS, sections were incubated in an avidin–peroxidase complex (PK-4001, Vectastain ABC kit, Vector Laboratories) for 45 minutes. Sections were washed 3 × 10 minutes in PBS. Staining was performed using nickel diaminobenzidine tetrahydrochloride (Ni-DAB) Chromagen (SK-4100, DAB Peroxidase Substrate Kit, 3,3′-diaminobenzidine, Vector Laboratories) for approximately 30 seconds to stain Fos-like products black. PBS was added immediately after desired stain was reached and sections were washed in 3 × 10 minutes in PBS to halt the Ni-DAB reaction. Sections were mounted on gelatin-coated slides (Fisherbrand Double Frosted Microscope Slides, Thermo Fisher Scientific Inc., Bridgewater, NJ, USA) and dehydrated with ethanol and xylenes prior to coverslipping with permount.

Imaging and Quantification of c-Fos Positive Nuclei

Coronal sections from area postrema (AP) and 4 rostrocaudal levels of the nucleus of the solitary tract (NTS) were analyzed per animal. The anterior–posterior levels were determined by coordinates from Bregma. The NTS areas consisted of anatomically matched sections from caudal (cNTS; −7.92 mm), at the level of the obex, corresponding to the posterior edge of the AP; medial (mNTS; −7.48 mm) at the maximal extent of the AP; intermediate (iNTS; −7.08 mm), anterior to the AP, corresponding to the maximal extent of the gelatinous subnucleus of the NTS; rostral (rNTS; −6.84 mm) consisting of the area rostral to the gelatinous nucleus and the caudal aspect of the medial vestibular nucleus on the dorsal boundary. Imaging was performed using an Olympus FSX-BSW imaging scope and FSX100 software (Olympus videoscope, Tokyo, Japan). Quantification was performed by identifying c-Fos positive black nuclei using Image J software system (NIH, Bethesda, MD, USA) image analysis software. Three anatomically matched tissue slices of each region (unilateral) of each mouse were used in data analysis. Cells were counted by 1 observer blinded to the experimental conditions.

Oral Glucose and Insulin Tolerance Tests

Oral glucose tolerance tests were performed at week 3, 8, and 16 of the diet intervention as previously described [4]. Mice (n = 15/group) were fasted in the morning for 6 hours and fasting blood glucose (t = 0 minutes) was measured. Mice were then administered D-dextrose (2 g/kg) dissolved in water via oral gavage, and blood glucose concentration was measured from tail-pricks after 15, 30, 60, 90, and 120 minutes using a glucometer (AlphaTRAK, Abbott Animal Health). An insulin tolerance test was performed after 15 weeks on diets. Mice (n = 8/group) were weighed and fasted overnight for 16 hours. Fasted mice were intraperitoneally injected with insulin (0.75 U/kg) and blood glucose was measured from tail pricks after 15, 30, 60, 90, and 120 minutes using a glucometer. Results are presented as mean blood glucose ± SD at

each timepoint, and as mean area under the blood glucose curve, calculated for each mouse.

Indirect Calorimetry

Volume of oxygen consumption (VO_2), carbon dioxide excretion (VCO_2), and physical activity were measured using the Comprehensive Laboratory Animal Monitoring System and Software (Oxymax-CLAMS, Columbus Instruments, Columbus, Ohio). Mice (n = 6-8/group) were acclimated for 24 hours in the Oxymax chamber, and measurements from each hour averaged over the following 48 hours were used for analysis. All data were normalized to body weight. Respiratory exchange ratio (RER) was determined by calculating VCO_2/VO_2. Physical activity is portrayed as ambulatory movements along the x-axis of the chamber (X_{amb}). X_{amb} includes nonrepetitive beam breaks during an interval and does not include repetitive breaks due to grooming movements. VO_2, non-protein RER and calorific value (CV) were used to calculate energy expenditure (kcal/min/kg body weight) over light and dark cycles, using the equation, $VO_2 \times CV = kcal$. CVs were calculated using the equation $CV = 3.815 + 1.232 * RER$, derived from empirical data from Graham Lusk's "The Elements of the Science of Nutrition" [37] Urinary nitrogen was not measured, but negligible protein oxidation was assumed in calculating total energy expenditure. Results are presented as mean VO_2 or $VCO_2 \pm$ SD per diet group over 24 hours, or as individual RER and energy expenditure per mouse.

Cholesterol and Lipid Analysis

Total cholesterol was detected in liver and serum via a fluorometric assay (Total Cholesterol Assay Kit; VWR; STA-384). Ten to 15 mg of frozen tissue was cut and homogenized in 200 µL chloroform: isopropanol: NP-40 (7:11:0.1). Extracted livers were diluted 2:3 and cardiac serum was diluted 1:100 in assay diluent prior to reading. Fluorescence was read by a ClarioStar spectrophotometer. Total lipids were detected in liver samples (300 mg) using Folch's method, as previously described [4].

Immunoassay Peptide Quantification

From the subset of mice used in 2.3 for neural activation assay, portal blood (n = 6/group) was collected into microfuge tubes and mixed with 50 µM dipeptidyl peptidase IV inhibitor (EMP Millipore, Billerica, MA) and immediately stored on ice for 30 minutes. Serum levels of total interleukin (IL)-6, tumor necrosis factor (TNF) α), GLP1, PYY, and leptin were evaluated using the Milliplex Map Mouse Metabolic Hormone Expanded Panel Kit (Catalog MMHE-44K Millipore, Billerica, MA, USA). Samples were assayed using a MagPix instrument (Luminex Corporation, Austin, TX, USA).

Tissue Gene Expression Analysis

mRNA was extracted from ileal tissue (30-60 mg) with RNeasy Plus Universal Mini Kit (QIAGEN) followed by RNA cleanup (Machery-Nagel, RNA purification kit). mRNA (5 µg) was reverse transcribed with random primers (High-Capacity cDNA Reverse Transcription Kit, Applied Biosystems), cDNA was diluted 1:3 in sterile ddH_20, and quantitative polymerase chain reaction (qPCR) was performed using TaqMan primers (Life Technologies, primer details are in Table 3 [34]) and TaqMan Fast Universal PCR Master Mix (2×), no AmpErase UNG (Life Technologies). Data were analyzed using $2^{-\Delta CT}$ method using hydroxymethylbilane synthase (*Hmbs*) as housekeeping gene for hepatic and hypothalamic tissue and 18S rRNA gene for ileal tissue.

Alanine Transaminase Assay

Using 20 µL of serum samples collected via submandibular bleed at week 15, alanine transaminase (ALT) assay was performed using Liquid ALT (SGPT) Reagent Set by Pointe Scientific Inc (REF: A7526-450; LOT 007901-168) per manufacturer protocol. Absorbance at 340 nm was read using a ClarioStar multimode plate reader.

LC-MS Quantification of Steroid Hormones

Steroid hormones were quantified by external calibration curves (0.001-5 µg/mL) with authentic standards (purity >95%) and corrected using internal standard (IS) calibration (see Table 4 [34] for analytes with abbreviations, suppliers, monoisotopic mass, ionization mode, cone voltage, retention time, and corresponding IS for calibration). Individual analyte stocks were pooled in a sampler vial to concentrations of 5 µg/mL and serially diluted to generate a calibration curve of 8 points ranging between 0.00156 and 5.0 µg/mL in 80% methanol. To reduce variability between runs, samples from HFD and HFD-GP groups were run in staggered fashion. Analytes were analyzed on a Water's Alliance e2695 high-performance liquid chromatography (HPLC) system coupled to a Water's Acquity QDA mass spectrometer equipped with an electrospray interphase. Analytes were separated in a Cortecs C18+ column (4.6 × 150 mm, 2.7 µm; Waters Milford, MA, USA) and gradient elution with 0.1% formic acid in water (solvent A) and 0.1% formic acid in acetonitrile (solvent B) at flow rate of 1 mL/min as follows: 0 to 30 minutes linear gradient from 65% to 35% B; 30 to 31 minute isocratic at 50% B; 31 to 31.10 step gradient to 35% B and 31.10 to 40 minutes isocratic at 35% B before returning to initial conditions at 60 minutes for the next analysis. The temperature of the column was maintained at 40 °C and the injection volume was 10 µL. Analytes were detected in full scan mode (electrospray interface +/−, scan range 100-1200 *m/z*) coupled with selective ion recordings. Detection and precision of the method is demonstrated elsewhere (Table 5 [34], which includes limit of detection, limit of quantification, and calibration curves generated from duplicate or triplicate runs of pure standards, and the coefficients of variation determined from standard quality controls). Calibration curves generated in each run were linear ($R^2 \geq 0.98$; Table 6 [34]). Matrix effects and recovery of IS in serum, liver, feces, and cecal matrices are provided elsewhere (Table 7 [34]).

Serum Steroid Hormones Extraction

Serum samples (50 µL) were placed in tubes containing 200 µL of evaporated steroid hormone internal standards (1 µg/mL; internal standards used included in Table 4 [34]), and 100 µL of acetonitrile was added and incubated at −20 °C for 1 hour to precipitate serum proteins. Samples were centrifuged at 16 000 rcf for 10 minutes. Supernatants were collected and loaded on Oasis Prime HLB Cartridges (Waters, Milford, MA, USA) to remove phospholipids.

Cartridges were subjected to a wash step (5% acetonitrile/95% water, v/v) and elution step (90% acetonitrile/10% water, v/v); these fractions were collected in separate tubes, evaporated, and resuspended in 200 µL of 50% methanol. Samples were filtered with Corning Costar Spin-X centrifuge tube filters Nylon membrane, pore size 0.22 µm for 1 minute at 16 000 rcf then transferred to 300-µL inserts in sampler vials for HPLC analysis. The recovery of IS after the column-purification step was 70% to 80%.

Liver Tissue Steroid Hormones Extraction

Frozen liver tissue (50-60 mg) was cut on dry ice and transferred into 2-mL bead beating tubes with 4 steel beads. Samples were homogenized in 300 µL of water using a genogrinder (Model 1600 MiniG Metuchen, NJ, USA) for 4 minutes. Homogenized tissue was transferred to tubes with 200 µL of predried internal standard (internal standard used included in Table 4 [34]). Protein precipitation step was performed with 1.1 mL 99.9% acetonitrile with 1% formic acid and placed on an orbital shaker for 1 hour at 4 °C. Samples were centrifuged at 13 000*g* for 15 minutes at 4 °C and supernatant was transferred to glass scintillation vials. The pellet remaining after centrifugation was resuspended in 1 mL of 80% methanol and sonicated for 1 minute with a cup-horn sonicator (Q700 Sonicator; Qsonica, LLC); 55% AMP, 30 second on, 59 second off, then a final 30 second on). Sonicated samples were centrifuged at 16 000*g* for 20 minutes at 4 °C and supernatants were pooled then dried under speed vacuum at room temperature overnight. Samples were resuspended in 200 µL 80% methanol + 0.1% formic acid, vortexed 2 minutes, and filtered through Corning Costar Spin-X centrifuge tube filters (Nylon membrane, pore size 0.22 µm) for 1 minute at 16 000*g*, then transferred into sampler vials with 300-µL inserts for HPLC analysis. Concentrations (µg/mg tissue) were determined by dividing final concentrations by frozen tissue weights used for extraction.

Fecal and Cecal Steroid Hormones Extraction

Feces from week 15 and cecal content collected at sacrifice at week 17 were stored at −80 °C until used. One milliliter of water was added to each sample and frozen prior to lyophilization (Freeze dryer, Labconco Corporation, Kansas City, OH, USA) then 15 to 30 mg was weighed and transferred into a tube containing 200 µL of dried internal standard (1 µg/mL). Samples were extracted twice in 1.5 mL of 80% methanol for 30 minutes at 4 °C, then centrifuged for 10 minutes at 13 000*g*. Samples were extracted twice, and supernatants were pooled then evaporated overnight at room temperature in a speed vacuum. Dried extracts were resuspended in 200 µL of 80% methanol, filtered with Corning Costar Spin-X centrifuge tube filters (Nylon membrane pore size 0.22 µm) for 1 minute at 16 000*g*, then transferred to 300 µL inserts in sampler vials for HPLC analysis. Recovery of internal standards after extraction was 70% to 90% for feces and 90% to 100% for cecal content. Concentrations (µg/mg dried content) were determined by dividing by lyophilized weights used for extraction.

Short Chain Fatty Acid Analysis

Fecal samples were collected and immediately placed onto dry ice then stored at −80 °C. SCFAs (ie, acetate, butyrate, propionate, valerate) and BCFAs (isobutyrate and isovalerate) concentrations were quantified by GC-MS using previously described methods [38].

16S rRNA Amplicon Sequencing

gDNA was extracted from fecal and cecal samples using DNeasy PowerSoil Pro Kit (QIAGEN, Venlo, Germany) and purified using NucleoSpin gDNA clean up kit (Machery Nagel, Switzerland). Samples were eluted with RNAase free water and stored at −80 °C. gDNA was extracted from feces and cecal content, diluted to 20 ng/uL, and submitted to Azenta Life Sciences (Piscataway, NJ, USA) for 16S V3-V4 rRNA amplicon (16SEZ service). Paired-end sequences were imported into QIIME2, demultiplexed, and quality filtered using the q2-demux plugin. Demultiplexed sequences were denoised, decluttered, and merged with DADA2 using q2-dada2 to generate amplicon sequence variants (ASVs) [39]. Before alignment, 8 base pairs (bps) were trimmed from the beginning of forward and reverse sequences. Forward sequences were not truncated while reverse reads were truncated at 240 bps; 82% to 86% of all sequences passed filtering and 67% to 80% were merged successfully. Unique features (ASVs) were aligned with mafft [40] (via q2-alignment) and used to construct a phylogeny with fasttree2 (via q2-phylogeny) [41]. Sequences were rarified to 21 265, to not exclude samples. α- and β-Diversity metrics (observed features, Faith's Phylogenetic Diversity [42], weighted UniFrac and unweighted UniFrac [43], Jaccard distance, and Bray–Curtis dissimilarity), and principle coordinate analyses were estimated using q2-diversity plugin. Taxonomy was assigned to ASVs using the q2-feature-classifier [44] and classify-sklearn Naive Bayes taxonomy classifier trained on the Greengenes_13_8 99% using the 16SEZ primers provided by Azenta Life Sciences.

qPCR Quantification of *Akkermansia muciniphila*

Akkermansia muciniphila was quantified in fecal and cecal samples, as previously described [4]. gDNA extracted from fecal or cecal samples was diluted to 2.5 ng/µL. *A. muciniphila* abundance relative to total bacteria and archaea was quantified by qPCR using *A. muciniphila* (AM1, AM2) and universal primer (U341F, U515R) sets [4]. Fecal and cecal total bacteria were based on concentrations (ng/µL) detected by universal primer.

Colonic Mucus Thickness

Colonic intestinal tissue sections (n = 3-4 mice/group) with digesta were fixed in methyl-carnoy immediately after extraction for 24-48 hours, to preserve the mucus layer. Sections were embedded in paraffin and then processed for staining using an Alcian Blue/Periodic Acid Schiff Stain Kit (ThermoFisher Scientific). Ten images were taken per cross-section at 20× magnification and 10 regions per image were quantified for thickness (totaling 100 measurements per mouse) using ImageJx (US National Institutes of Health, Bethesda, MD; National Center for Microscopy and Imaging Research: ImageJ Mosaic Plug-ins, RRID:SCR_001935). Mucus thickness is presented as thickness ± SD (µm) of each mouse.

Intestinal Paracellular Permeability

An intestinal paracellular permeability test was performed at week 15 of the diet intervention. Starting at 6 AM (1 hour

before the beginning of the light cycle) mice (n = 6/group) were food-fasted in empty cages for 6 hours prior to testing. Mice were water-fasted for 2 hours. After the food and water fast, baseline blood samples were collected via submandibular bleeds while mice were anesthetized with isoflurane. Mice were orally administered an 80 mg/kg dose (~150 µL solution in sterile 1× PBS) of 4 kDA fluorescein isothiocyanate (FITC) dextran (Sigma-Aldrich) and blood was collected 4 hours post gavage. Blood samples were collected with anticoagulant (25% v/v acid-citrate dextrose solution) followed by centrifugation at 2000*g* for 10 minutes to isolate plasma. Samples were diluted 1:4 in 1× phosphate buffer solution (PBS) and fluorescence of technical duplicates were determined in a multimode plate reader (Clariostar, BMG) at 530 nm with excitation at 488 nm. Serially diluted FITC-Dextran in plasma was used to establish a standard curve. Samples were corrected for baseline fluorescence. The plasma concentration of FITC-dextran (mean ± SD, µg/mL) for each mouse 4 hours after oral gavage was used to evaluate intestinal permeability.

Statistical Analysis

Analyses were conducted and graphed using Prism 8.0.2 (GraphPad Software, La Jolla, CA, USA). Normality of data was determined by Shapiro–Wilks test. Outliers were removed using ROUT's test (Q = 1%). Significant differences for metabolic phenotypes were assessed via 2-way analysis of variance (ANOVA) (where time was a factor) or parametric 1-way ANOVA or nonparametric Kruskal–Willis test followed by Dunnett's post hoc test using the HFD group as a control so only 1 factor (ie, % fat or GP supplementation) was assessed in each comparison. For gene expression, metabolite analyses, and immunoassays the difference between HFD and HFD-GP groups was assessed by unpaired, 2-tailed, Student's t test or for nonparametric data, a Mann–Whitney test. $P < .05$ was considered significant. Statistical analysis of α- and β-diversity metrics was calculated using QIIME 2. ADONIS and permutation analysis were conducted using R Studio V.3.4.2 (R Studio Software, Boston, MA, USA). The Galaxy web application was used to perform LefSe differential analysis and to plot linear discriminant analysis effect size (huttenhower.sph.harvard.edu/lefse). Graphs were created using Prism 8.0.2 or Origin (Pro), Version 2019b (OriginLab Corporation, Northampton, MA, USA).

Results

GP Supplementation Attenuated HFD-Induced Weight Gain

Male C57BL/6J mice were fed LFD, HFD, or HFD supplemented with 0.5% GP (HFD-GP) for 17 weeks. The LFD group was included mainly to track HFD-induced imbalances to body mass, energy expenditure, and glucose handling. The mean daily food intake of the 3 groups (LFD: 2.91 ± 0.21 g, HFD: 2.85 ± 0.27 g, HFD-GP: 2.94 ± 0.29 g/day) was similar for most timepoints over the 17-week period (Fig. 1A). Due to higher caloric density, mice fed HFD, or HFD-GP consumed more calories per day than LFD-fed mice (Fig. 1B). Mice in the HFD-GP group ingested approximately 30 mg polyphenols (gallic equivalents) per day, of which 21.3 mg were proanthocyanidins. Confirming the obesogenic effect of HFD, LFD-fed mice had lower body weight gain, liver weight, hepatic lipids, and fat to lean mass ratio after 15 weeks

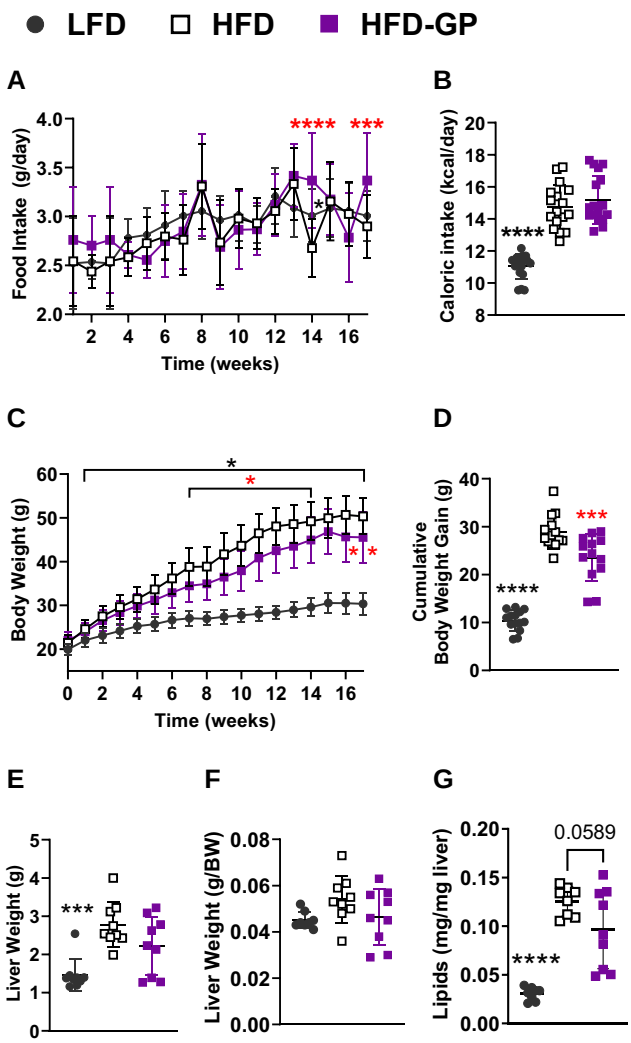

Figure 1. Effects of GP supplementation on caloric intake, body weight, and liver weight and lipid accumulation. (A) Weekly food intake (significant ANOVA results were obtained for time, $F(5331, 106.6) = 26.77$, $P < .0001$), diet, $F(2, 20) = 4.897$, $P = .0186$, and a time × diet interaction, $F(46, 460) = 3.552$, $P < .0001$). (B) Cumulative caloric intake (n = 15/group). (C) weekly body weight (significant ANOVA results were obtained for time, $F(2792, 106.3) = 633.4$, $P < .0001$, diet, $F(2, 39) = 70.63$, $P < .0001$, and a diet × time interaction, $F(34, 647) = 57.47$, $P < .0001$). (D) Cumulative body weight gain from baseline to week 17 (n = 15/group). (E) Liver weight at necropsy. (F) Weight normalized to body weight. (G) Lipid content (n = 9/group). All values are presented as mean of diet group ± SD. Symbols in scatter plots represent individual animals. Line graphs present the mean per diet group over time. Significant differences were determined by 2-way ANOVA where time and diet were factors, or otherwise a 1-way ANOVA (or for nonparametric data a Kruskal–Wallis test) followed by Dunnett's post hoc test with HFD group set as control. Black asterisks indicate statistically significant values between HFD and LFD-fed mice, and red asterisks indicate statistically significant values between HFD and HFD-GP-fed mice. $*P < .05$, $**P < .01$, $***P < .001$, $****P < .0001$. Numerical P values are indicated when $.05 < P < .1$.

(Fig. 1C-1G; Fig. 3A, B [34]). Compared with HFD-fed mice, GP supplementation attenuated HFD-induced body weight gain starting at week 6 of the diet intervention (Fig. 1C) and reduced cumulative body weight gain over the 17 weeks diet intervention (Fig. 1D), consistent with prior data [4]. HFD and HFD-GP groups had similar body composition (Fig. 3A, B [34]) and similar liver and serum cholesterol levels at endpoint (Fig. 3C, D [34]). HFD-fed and HFD-GP

groups had similar liver weight ($P = .12$), liver weight normalized to body weight ($P = .17$), and a trending decrease in liver lipids ($P = .06$; Fig. 1E-1G). As previously [5], GP supplementation did not alter hepatic gene expression of fat oxidation gene *Cpt1a* (Table 8 [34]); therefore, this trend of lower hepatic lipids could not be attributed to altered expression of lipolytic genes.

GPs Did Not Alter Glucose Metabolism

HFD feeding impaired glucose handling, as evidenced by reduced oral glucose tolerance and insulin sensitivity, and increased serum insulin concentrations compared with LFD-fed mice (Fig. 4A-C [34]). In our previous 12-week study, male C57BL/6 mice fed HFD supplemented with 1% GPs (twice the dose of GPs used in this study) had improved glucose tolerance compared with HFD-fed mice after 6 and 9 weeks of supplementation [4]. Here, GPs did not affect oral glucose tolerance throughout the diet intervention or insulin sensitivity at week 15 (Fig. 4A, B [34]). These results indicate that the lower 0.5% dose of GPs was ineffective for correcting HFD-induced glucose intolerance. Nonetheless, 0.5% GP supplementation resulted in other metabolic improvements.

Portal blood levels of GLP-1 were similar in LFD, HFD, and HFD-GP groups (Fig. 4C [34]), indicating that disruption to glucose regulation on a HFD was due to changed levels of this glucose regulating incretin. Despite unchanged glucose tolerance and GLP-1 levels, expression of regulatory genes was altered by GPs (ie, lower ileal gene expression of *Gcg* and a trending lower expression of *Glpr* ($P = .07$) compared with HFD-fed mice) (Table 8 [34]). Expression of prohormone convertase 1/3 (*Pcsk1*; required for cleavage of proglucagon into GLP-1 and GLP-2) was unchanged (Table 8 [34]).

GP Did Not Affect Hindbrain Sensitivity to Glucose

To test whether GP supplementation may increase central glucose sensitivity, c-Fos staining was performed on the dorsal vagal complex (ie, the nucleus of the tractus solitarius [NTS] and the area postrema [AP]) after oral glucose administration. C-Fos is recognized as a specific marker of neuronal activity as it is often expressed when neurons fire action potentials, and expression is increased in response to various pathological or physiological stimuli, including glucose [45]. The number of c-Fos positive neurons in the NTS was increased in 3 of 6 GP-supplemented mice, but statistically HFD and HFD-GP groups had similar numbers of c-Fos positive neurons in NTS and AP (Fig. 5A-C [34]). Thus, the GP dose utilized in this study did not significantly alter hindbrain sensitivity to glucose.

GP Supplementation Prevented HFD-Induced Reductions to Energy Expenditure

To investigate how GP supplementation lowered HFD-induced weight gain, metabolic rate was assessed by indirect calorimetry. Measured volumes of oxygen (VO_2) consumed, and carbon dioxide (VCO_2) produced indicate rates of cellular respiration, and in turn metabolic rate. Contributing factors to cellular respiration include body size, body composition, thermogenesis, gender, age, physical activity, and hormonal status [46]. As mice are nocturnal, their metabolic rate peaks during the night and declines during the day. Compared with HFD-fed mice, at week 15 GP-supplemented mice consumed more O_2 and emitted more CO_2 over several hours of the night, leading to increase energy expenditure (Fig. 2A-2C). The average energy expenditure during resting hours (daytime) was compared with the average energy expenditure during waking hours (nighttime) within diet groups. Mice within the LFD and HFD-GP groups showed significantly increased energy expenditure at nighttime compared with daytime hours ($P < .001$), but HFD-fed mice had similar energy expenditure at nighttime and daytime ($P = .1764$; Fig. 2D) suggesting GP supplementation may protect against HFD-induced blunting of the circadian oscillations of energy expenditure. Due to greater oxygen requirements of fat oxidation, metabolism of fat requires greater energy expenditure. Respiratory exchange ratio (RER) was calculated to assess macronutrient utilization, which is increased during carbohydrate metabolism (RER = 1) and reduced during fat metabolism (RER = 0.7); energy losses to protein metabolism are not considered in these calculations. As expected, HFD-based groups metabolized significantly more fat than the LFD-group (Fig. 2E). Compared with HFD-fed mice, GP supplemented mice had similar RER and comparable fat oxidation (Fig. 2E). Physical activity was similar in HFD and HFD-GP groups, which both had lower physical activity than LFD-fed mice over 9 timepoints (Fig. 2F). RER or physical activity could therefore not explain increased energy expenditure in the HFD-GP group relative to HFD-fed mice.

GP Supplementation Increased Circulating and Hepatic CORT and Impacted CORT-Related Gene Expression

GP supplementation had increased serum CORT levels in HFD-fed mice in both cardiac serum and liver tissue (Fig. 3A and 3B), suggesting increased HPAA activity. CORT levels were similar between HFD and LFD-fed mice (Fig. 6 [34]), suggesting that without GP supplementation, HFD-fed mice could not maintain upregulated HPAA activity needed to offset weight gain. We measured enzymes which activate and clear CORT as well as CORT metabolites to determine the role of peripheral tissues in regulating CORT levels. Hepatic 11β-HSD1 (encoded by *Hsd11b1*) converts 11-dehydrocorticosterone (11-DH-CORT) to its active form as CORT [17]. Hepatic enzymes 5α- and 5β-reductase (encoded by *Akr1d1* and *Srd5a1*, respectively) are involved in CORT clearance via conversion to the tetrahydrometabolites 5α-tetrahydrocorticosterone (5α-TH-CORT) and 5α-dihydrocorticosterone (5α-DH-CORT), which have reported functions related to decreased neuronal excitability that can reduce pain and inflammation [47, 48]. Hepatic 11-DH-CORT concentrations were not significantly changed (Fig. 3B) and *Hsd11b1* mRNA levels only trended lower in HFD-GP than in HFD-fed mice ($P = .115$; Fig. 3C). 5α-TH-CORT and 5α-DH-CORT concentrations were unchanged, though hepatic gene expression of *Akr1d1* and *Srd5a1* responsible for production of these tetrahydrometabolites was increased (Fig. 3C). Compared with HFD-fed mice ileal *Hsd11b1* gene expression was significantly reduced in GP supplemented mice, suggesting GPs may influence CORT homeostasis in the intestine (Fig. 3D). 11-DH-CORT, 5α-TH-CORT and 5α-DH-CORT were not detected in cardiac serum.

GP supplementation did not significantly affect gene expression of glucocorticoid receptor *Nr3c1* in liver or hypothalamic tissue (Table 8 [34]). Compared with HFD controls, GP-supplemented mice had a trending increase in hypothalamic mRNA levels of *Crh* ($P = .12$; Fig. 3E), suggesting hypothalamic signaling for CORT production may be upregulated.

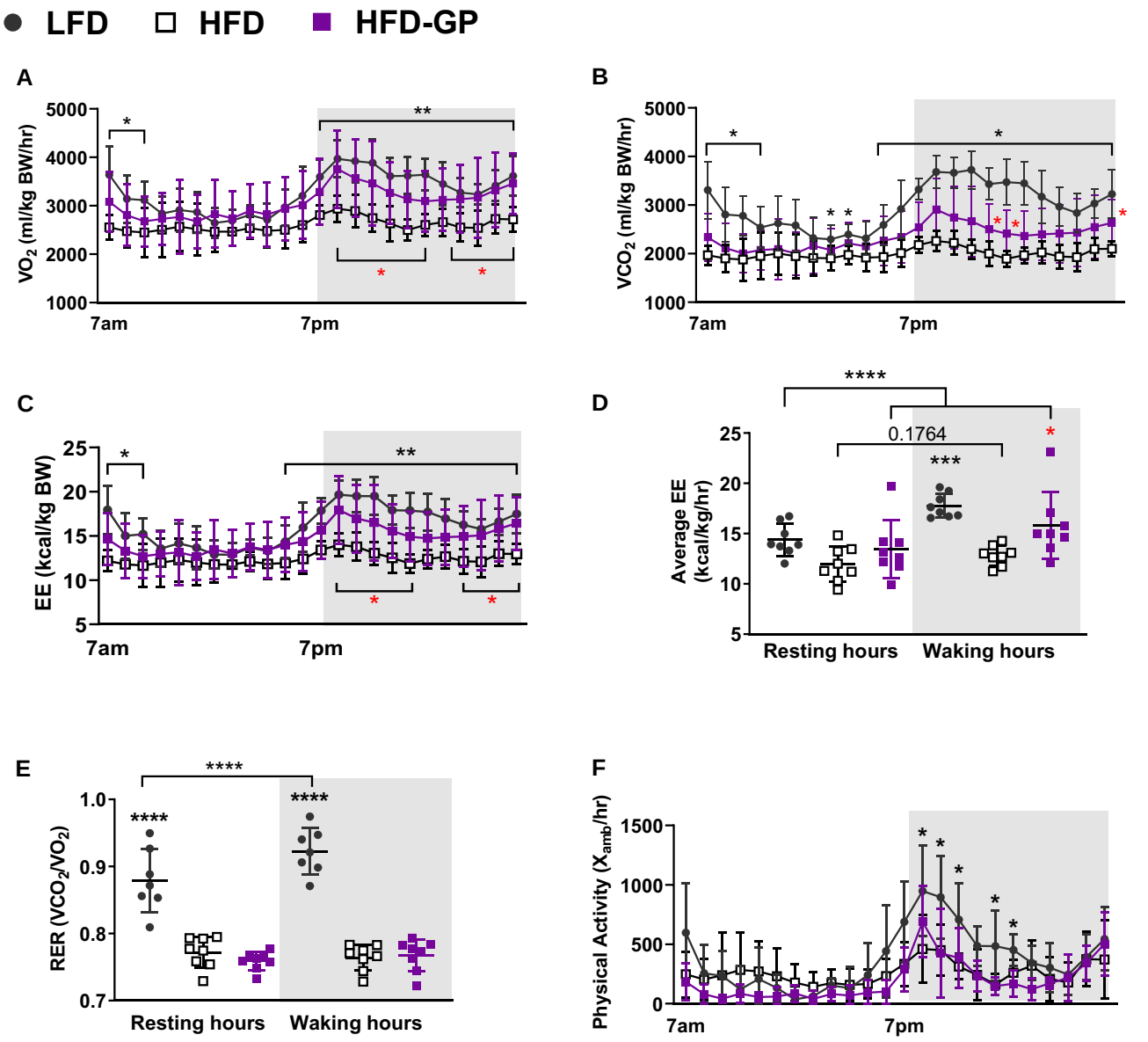

Figure 2. Effects of GPs on metabolic rate. Results from indirect calorimetry performed at week 15 measuring (A) volume of oxygen (VO_2) consumed (significant ANOVA results were obtained for time, $F(23, 480) = 6.748$, $P < .0001$ and diet, $F(2480) = 89.14$, $P < .0001$) (B) volume of carbon dioxide (VCO_2) exhaled (significant ANOVA results were obtained for time, $F(5392, 107.8) = 23.58$, $P < .0001$, diet, $F(2, 20) = 14.15$, $P = .0001$, mouse, $F(20, 460) = 49.04$, $P < .0001$, and a time × diet interaction, $F(46, 460) = 5440$, $P < .0001$) (C) energy expenditure (EE) (significant ANOVA results were obtained for time, $F(23, 504) = 7.844$, $P < .0001$ and diet, $F(2, 504) = 115.6$, $P < .0001$), and (D) paired comparison of average EE of resting (7 AM-6 PM) compared with waking (7 PM-6 AM) hours (significant ANOVA results were obtained for time, $F(2, 21) = 8.826$, $P = .0017$, diet, $F(1, 21) = 6.533$, $P = .0062$ and a diet × time interaction, $F(2, 21) = 8.826$, $P = .0017$) (E) resting exchange ratio (RER) at resting and waking hours (significant ANOVA results were obtained for time, $F(1, 20) = 12.64$, $P = .0002$, diet, $F(2, 20) = 63.17$, $P < .0001$ and a time × diet interaction $F(2, 20) = 12.94$, $P = .0002$), and (F) physical activity, averaged per diet group (n = 7-8/group; significant ANOVA results were obtained for time, $F(6.073, 121.5) = 17.54$, $P < .0001$, diet, $F(2, 20) = 6.434$, $P = .007$, mouse, $F(20, 460) = 7.279$, $P < .0001$, and a time × diet interaction, $F(46, 460) = 2.592$, $P < .0001$). All values are presented as mean of diet group ± SD for line graphs or individual animal ± SD. Each symbol represents an individual mouse in scatter plots. Statistically significant differences were determined by 2-way ANOVA where diet and time were factors, or otherwise a parametric 1-way ANOVA followed by Dunnett's post hoc or nonparametric (Kruskal–Wallis) test followed by Dunnett's post hoc test, using the HFD group as a control group. Unpaired Student t-tests, or Mann–Whitney tests for nonparametric data, were performed to compare resting vs waking hour values within diet groups. Black asterisks indicate statistically significant values between HFD and LFD-fed mice, and red asterisks indicate statistically significant values between HFD and HFD-GP-fed mice. $*P < .05$, $**P < .01$, $***P < .001$, $****P < .0001$. Numerical P values are indicated when $.05 < P < .1$. BW, body weight; EE, energy expenditure.

HFD feeding was shown to increase expression of hypothalamic proopiomelanocortin, which was further enhanced by adrenalectomy which abrogates CORT production [49]. Compared with HFD-fed mice, GP supplemented mice showed a trending decrease in hypothalamic *Pomc* mRNA ($P = .09$; Fig. 3E), which may contribute to the observed increase in circulating CORT. Compared with HFD-fed mice, the HFD-GP group had decreased expression of gonadotropin releasing hormone (*GnRH*), a marker of the hypothalamic pituitary gonadal (HPG) axis (Fig. 3E). The HPAA inhibits the HPG axis to conserve energy [50]; therefore, a GP-induced reduction to *GnRH* is consistent with GP supplementation promoting HPAA activity leading to reduced HPG-axis activity.

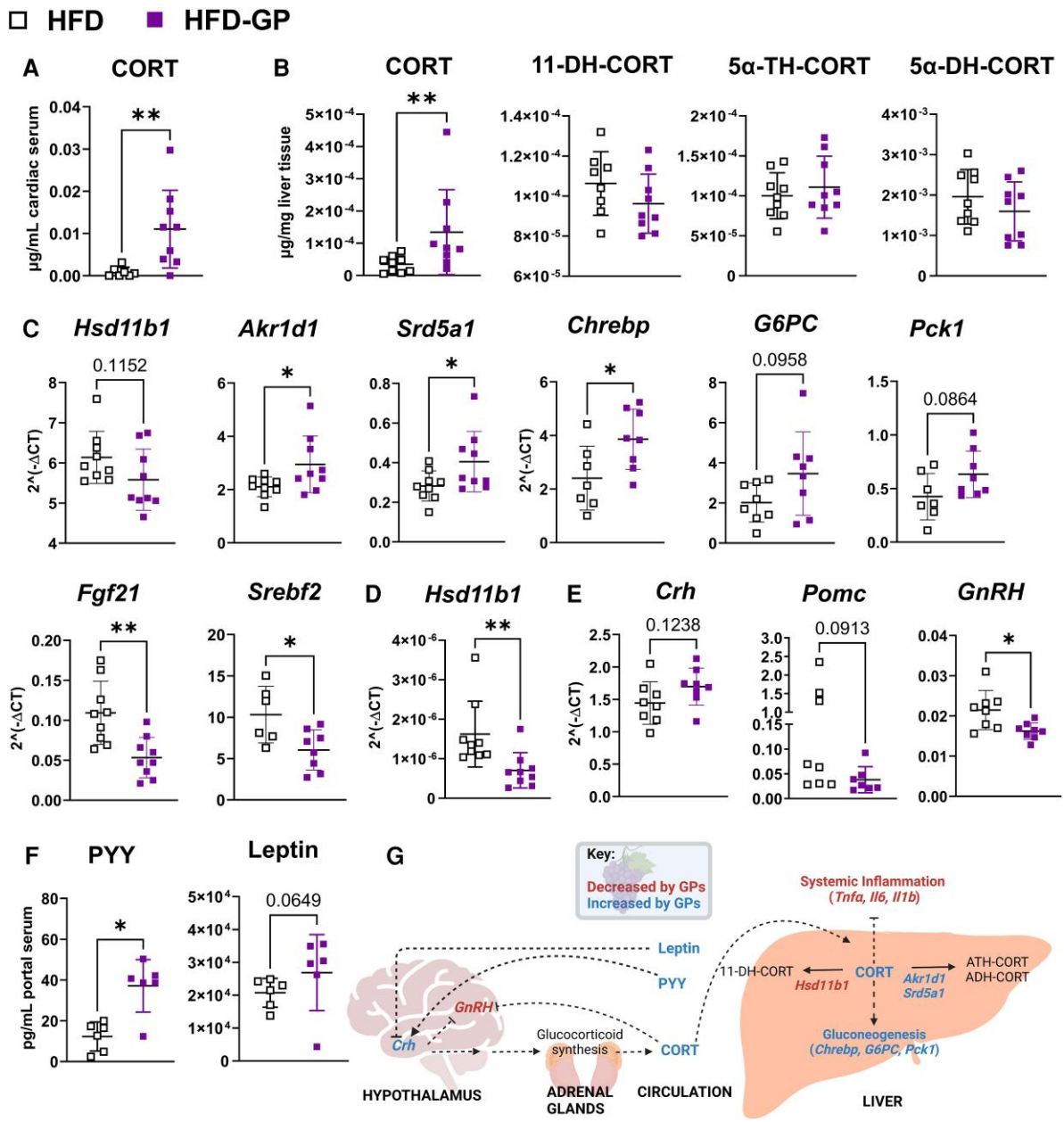

Figure 3. Markers of HPAA activity. LCMS detection of concentrations of corticosterone (CORT) in (A) serum, and (B) liver along with detected inactive CORT (11-DH-CORT), and CORT metabolites, 5α-TH-CORT and 5α-DH-CORT (n = 9/group). Gene expression of (C) hepatic *Hsd11b1* (11β-Hydroxysteroid dehydrogenase type 1), *Akr1d1* (5β-reductase), *Srd5a1* (5α-reductase), *Nr3c1* (glucocorticoid receptor), *Lepr* (leptin receptor), G6Pc (glucose-6-phosphatase), *Pck1* (phosphoenolpyruvate carboxykinase 1), *Chrebp* (Carbohydrate-responsive element-binding protein), *Srebf2* (sterol regulatory element-binding protein), and *Fgf21* (fibroblast growth factor 21), and (D) Ileal *Hsd11b1*, and (E) hypothalamic *Crh* (corticotropin-releasing hormone), *Pomc* (proopiomelanocortin), and *GnRH* (gonadotropin-releasing hormone) (n = 7-8/group). (F) Serum concentrations of PYY and leptin in portal blood measured by an immunoassay (n = 6/group). (G) Schematic of effects of GP supplementation on markers of HPA-axis activity created with Biorender.com. Unpaired Student t tests or Mann–Whitney test (for nonparametric data) were performed. $*P < .05$, $**P < .01$, $***P < .001$, $****P < .0001$; Numerical P values are indicated when $.05 < P < .15$. Each symbol in scatter plots represents a single animal.

GP Supplementation Upregulated Markers of Hepatic Gluconeogenesis

The HPAA promotes gluconeogenesis to satisfy increased energy needs during waking hours and periods of stress [13, 14]. Compared with HFD-fed mice, mice fed HFD-GP had increased hepatic gene expression of carbohydrate-responsive element-binding protein (*Chrebp*) and a trending increase in expression of glucose-6-phosphatase (*G6pc*) and phosphoenolpyruvate carboxykinase 1 (*Pck1*) (Fig. 3C). In vitro studies showed that ChREBP could reduce lipogenic sterol regulatory element-binding protein (SREBP2) levels via direct binding and ubiquitination [51]. Consistent with increased *Chrebp* expression, GP supplemented mice also had reduced hepatic mRNA levels of *Srebf2* (Fig. 3C). ChREBP regulates hepatic production of fibroblast growth factor 21 (FGF21), a regulator of energy homeostasis and carbohydrate metabolism that suppresses hepatic expression of SREBP2 [52, 53] in association with reduced hepatic steatosis and increased energy expenditure [54]. Mice fed a high-fat, high-sucrose diet showed increased *Fgf21* mRNA levels in liver and WAT, increased

FGF21 in circulation, but impaired FGF21 signaling [55]. Compared with HFD-fed mice, GP-supplemented mice had decreased hepatic mRNA levels of *Fgf21* (Fig. 3C), suggesting enhanced ChREBP-FGF21 signaling and increased FGF21 sensitivity.

GP Supplementation Induced Hormones that Promote Energy Homeostasis

CORT increases leptin production, which in turn works by negative feedback to suppress the HPAA. Leptin is secreted by adipocytes and normally functions to signal energy excess to the brain, which responds by increasing energy expenditure and triggering release of the anorexigenic enteroendocrine hormone, peptide YY (PYY) [56]. Rats with HFD-induced obesity were previously shown to have reduced CRH and CORT levels while leptin levels increased, suggesting an uncoupling of CORT and leptin feedback [10]. HFD-fed mice had lower PYY levels than LFD-fed mice, suggesting reduced enteroendocrine activity (Fig. 6A [34]). Compared with LFD, leptin levels were significantly elevated in portal blood of HFD-fed mice (Fig. 6A [34]) consistent with their increased fat mass (Fig. 3A [34]), Compared with HFD-fed mice, the portal blood of GP-supplemented mice had increased levels of PYY and a trending increase in leptin levels ($P = .065$; Fig. 3F), suggesting GPs can increase enteroendocrine activity and stimulate adaptation to HFD. HFD and HFD-GP groups showed similar ileal mRNA levels of *Pyy* (Table 8 [34]), suggesting GPs modulate PYY release, rather than gene expression. Hepatic leptin receptor (*Lepr*) mRNA levels were similar between HFD and HFD-GP groups (Table 8 [34]). These results suggest GPs may increase enteroendocrine activity and preserve coupling between leptin and PYY signaling on a HFD.

GP Supplementation Reduced Markers of Inflammation in the Liver and Intestine

Previously, relative to HFD, mice fed HFD containing 1% GP had reduced serum levels of TNFα and IL-6 as well as ileal mRNA levels of these cytokines [4]. Here, compared with HFD-fed mice, mice fed HFD with 0.5% GP had reduced ileal gene expression of *Il6* and a trending decrease in *Tnfa*, reduced hepatic *Il1b* and trending reductions in *Tnfα* and *Il6*, and unchanged hypothalamic expression of *Tnfα*, *Il6*, or *Il1b* or concentrations of TNFα and IL-6 in portal blood (Fig. 4A-D). Compared with LFD-fed mice, HFD-fed mice showed a trend of increased TNFα levels in portal blood ($P = .0649$), and no change in IL6 or ALT levels (Fig. 6A, B [34]). Compared with HFD-fed mice, ALT levels in cardiac serum were higher in GP-supplemented mice though still within normal range (Fig. 4E). Elevated ALT (>40 U/L serum) can be a symptom of liver injury from fatty liver, cirrhosis, cancer, and ischemia but could also indicate increased gluconeogenesis independent of liver injury [57]. In conjunction with reduced markers of inflammation and increased markers of gluconeogenesis, increased ALT in the HFD-GP group is more likely evidence for a gluconeogenic state rather than hepatocellular injury.

GP Supplementation Did Not Significantly Alter Short Chain Fatty Acids

In a prior study, wild-type male mice fed a butter fat and sucrose-rich Western diet supplemented with 1% GP resulted in less butyrate and a lower acetate:propionate ratio in colon content, which was hypothesized to reduce hepatic lipogenesis [5]. In this study, compared with HFD-fed mice, mice fed HFD-GP showed a trend of reduced fecal acetate ($P = .06$; Fig. 7 [34]).

GP Supplementation Altered BA Composition in Serum, Liver, Cecum, and Feces

Primary BA (PBA) are released postprandially to aid in lipid absorption, after which some may be converted to secondary BA (SBA) by gut bacteria prior to reabsorption. PBA and SBA species (listed in Table 4 [34]) were quantified in serum, liver, cecum, and feces to investigate the effects of GP supplementation on BA composition, microbial metabolism, and excretion. Compared with HFD-fed mice, cardiac serum of GP-supplemented mice had reduced pools of total bile acids (TBAs), PBAs, SBAs, and unconjugated Bas (Fig. 5B, left and right panels), as well as a reduced fraction of SBA and increased fraction of PBA relative to TBA pool (Fig. 5B, middle panel). Specifically, GP supplementation reduced cholic acid (CA), chenodeoxycholic acid (CDCA), α-muricholic acid (α-MCA), ωMCA, and tauro-ωMCA (TωMCA) and increased taurocholic acid (TCA) (Fig. 5A and Table 1). PBA could be reduced in serum due to reduced hepatic BA synthesis, while both PBA and SBA levels could be reduced due to increased hepatic BA excretion or reduced intestinal BA reabsorption. Though still possible, levels of PBA or TBAs were not affected in hepatic tissue to suggest changed BA synthesis in GP-supplemented mice; however, a trending reduction in the pool of hepatic SBAs ($P = .06$; Fig. 5C, left panel), could be due to reduced reabsorption or reduced bacterial synthesis. GP supplementation decreased hepatic levels of TβMCA, glycoursodeoxycholic acid (GUDCA), taurohyodeoxycholic acid (THDCA), and TωMCA (Table 1) though the summed levels of conjugated Bas and unconjugated BA in liver tissues remained similar between HFD and HFD-GP groups (Fig. 5C, right panel).

There was no significant difference between HFD and HFD-GP groups with respect to cecal or fecal PBA, SBA, TBA, conjugated or unconjugated BA concentrations (Fig. 5D and 5E), suggesting that BA excretion was not upregulated by GP supplementation. GP supplementation increased cecal levels of TCA, TCDCA, TUDCA, TβMCA, taurodeoxycholic acid (TDCA), THDCA, and taurolithocholic acid (TLCA; Fig. 5A and Table 1). Compared with HFD-fed mice, GP-supplemented mice had less hyocholic acid (HCA) in both cecal content and feces, while CA and ursodeoxycholic acid (UDCA) were reduced in feces only (Fig. 5A and Table 1). Overall, changes to BA profile in GP-supplemented mice provide evidence for altered BA metabolism and transfer, suggesting changes to gene expression of BA regulating genes.

GP-Supplemented Mice Exhibited Markers of Intestinal Farnesoid X Receptor Inhibition

Activation of BA receptors farnesoid X receptor (FXR, encoded by nuclear receptor subfamily 1, group H, member 4, *Nr1h4*), constitutive androstane receptor (CAR, encoded by *Nr1i3*), and Takeda-G-protein receptor-5 (TGR5) lead to gene expression changes that limit BA synthesis and increase BA flow to prevent cytotoxic BA accumulation in hepatic and intestinal cells [58, 59]. FXR-regulated genes and GP effects are summarized in Fig. 6A to display how GPs could

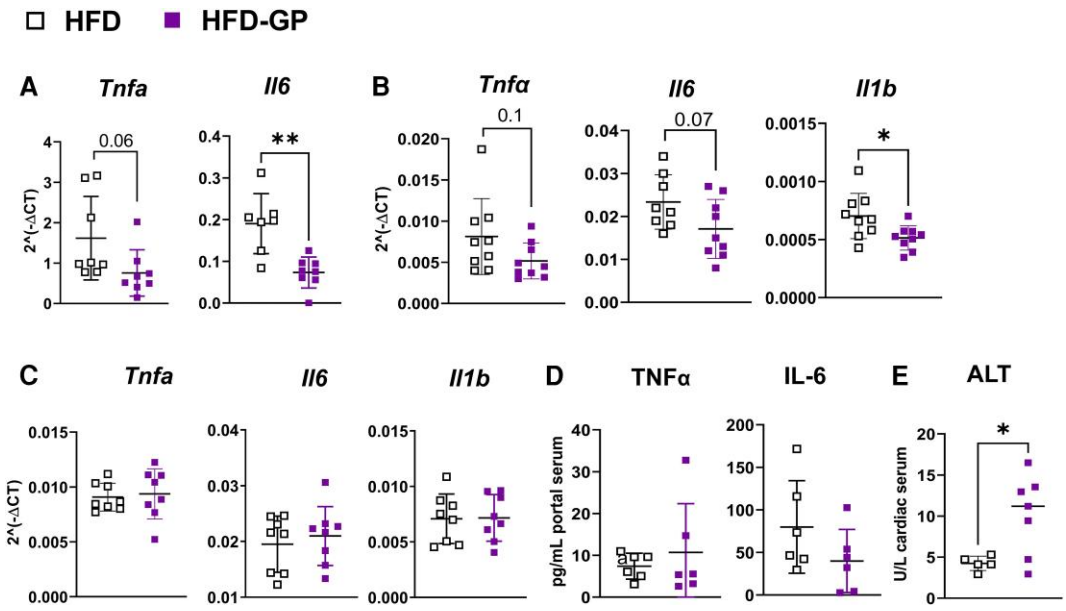

Figure 4. Effects of GP supplementation on inflammation. Gene expression of inflammatory cytokines detected in (A) ileal, (B) liver, and (C) hypothalamic tissue (n = 8-9/group). Serum concentrations of (D) TNFα and IL-6 in portal blood (n = 6/group), and (E) alanine transferase (ALT) in cardiac blood (n = 5-7/group). Values are presented as mean ± SD, and each symbol represents an individual mouse. Unpaired Student t tests or Mann–Whitney tests, for nonparametric data, was performed. $*P < .05$, $**P < .01$, $***P < .001$, $****P < .0001$; Numerical *P*-values are indicated when $.05 < P < .1$.

direct BA flow away from systemic circulation. HFD-GP–fed mice had a trending reduction in ileal *Fxr* ($P = .06$) and ileal and hepatic *Shp* ($P = .07$) (Fig. 6B and 6C), consistent with GP-induced inhibition of intestinal FXR, seen previously in GP supplemented leptin-deficient *db/db* mice [9]. Ileal *Fgf15* and hepatic *Fxr* were unaffected by GP supplementation (Fig. 6B and 6C). Compared with HFD-fed mice, GP-supplemented mice showed increased hepatic expression of *Cyp7a1* and a trending increase in *Cyp27a1* ($P = .08$; Fig. 6C), supporting reduced FXR activity. Thus, reduced PBA levels in circulation of GP-supplemented mice (Fig. 5B) were not likely due to downregulated hepatic BA synthesis. We subsequently hypothesized that the GP-induced increase in BA synthesis might reduce hepatic cholesterol accumulation; however, liver and serum cholesterol concentrations were similar in HFD and HFD-GP groups (Fig. 3C, D [34]). While total cholesterol concentrations were not affected by GP, cholesterol like high-density lipoprotein could have been increased in place of the "bad" low-density lipoprotein that contributes to plaque formation, and thus warrants further investigation.

Consistent with reduced FXR activation, GP-supplemented mice had reduced ileal levels of *Ibabp* and *Ostβ* as well as hepatic *Abcc3 and* increased hepatic *Oatp1* (Fig. 6B and 6C), indicative of reduced BA transfer from enterocytes and hepatocytes into portal and systemic circulation [58, 60]. Compared with HFD-fed mice, GP supplementation did not affect ileal *Ostα*, *Abcc3*, *Slc10a2*, and *Tgr5* or hepatic *Ostα*, *Ostβ*, *Slc10a1*, and *Abcb11* (Table 8 [34]). GP supplementation increased hepatic mRNA levels of *Nr1i3* (Fig. 6C), suggesting upregulated detoxification of endogenous and exogenous chemicals, including detoxification of Bas via metabolism or conjugation [61, 62]. Bas that enter hypothalamic neurons via ASBT modulate the HPAA [30]. GP supplementation did not affect hypothalamic mRNA levels for ASBT (Table 8 [34]), though whether GPs affect BA levels in hypothalamic neurons remains to be investigated.

GP Supplementation Did Not Alter Intestinal Permeability Mucus Layer

HFD-fed mice that were orally administered bacterium *A. muciniphila* were previously shown to have increased intestinal mucus thickness in association with improved metabolic phenotypes [63]. Mice fed HFD supplemented with 1% GP developed a bloom of *A. muciniphila* with almost complete redistribution of the colonic mucus layer into the intestinal lumen and a reduction in inflammatory markers [64]. Compared with HFD-fed mice, mice fed HFD supplemented with 0.5% GP did not show any reduction in the colonic mucus layer thickness or in intestinal permeability (Fig. 8A-C [34]). GP supplementation appears to affect the intestinal mucus layer in a dose-dependent manner and metabolic improvements are independent of mucus layer thickness.

GP Supplementation Altered the Gut Microbial Community

16S rRNA amplicon sequencing was performed to assess cecal microbial communities after 17 weeks of HFD or HFD-GP intervention. A total of 281 ASVs were identified over different taxonomic levels. The microbial communities of HFD and HFD-GP groups were similar in terms of α-diversity metrics (Richness, Evenness, Faith phylogenetic diversity; Fig. 7A), indicating supplementation with 0.5% GP did not alter the number of different microbial species and their distribution (aka evenness). Principle coordinate analysis on weighted UniFrac, a β-diversity metric which accounts for both bacterial presence and abundance, showed notable dissimilarities between gut microbial communities of HFD and HFD-GP groups ($R = 0.75$, $P = 9.99 \times 10^{-5}$) while unweighted UniFrac, measuring only presence of taxa, showed weaker but still significant effects ($R = 0.26$, $P = .017$; Fig. 7B and 7C). Unifrac analyses indicate that while gut bacteria in HFD and HFD-GP groups have moderate phylogenetic differences, GPs mainly alter the relative abundance of different taxa.

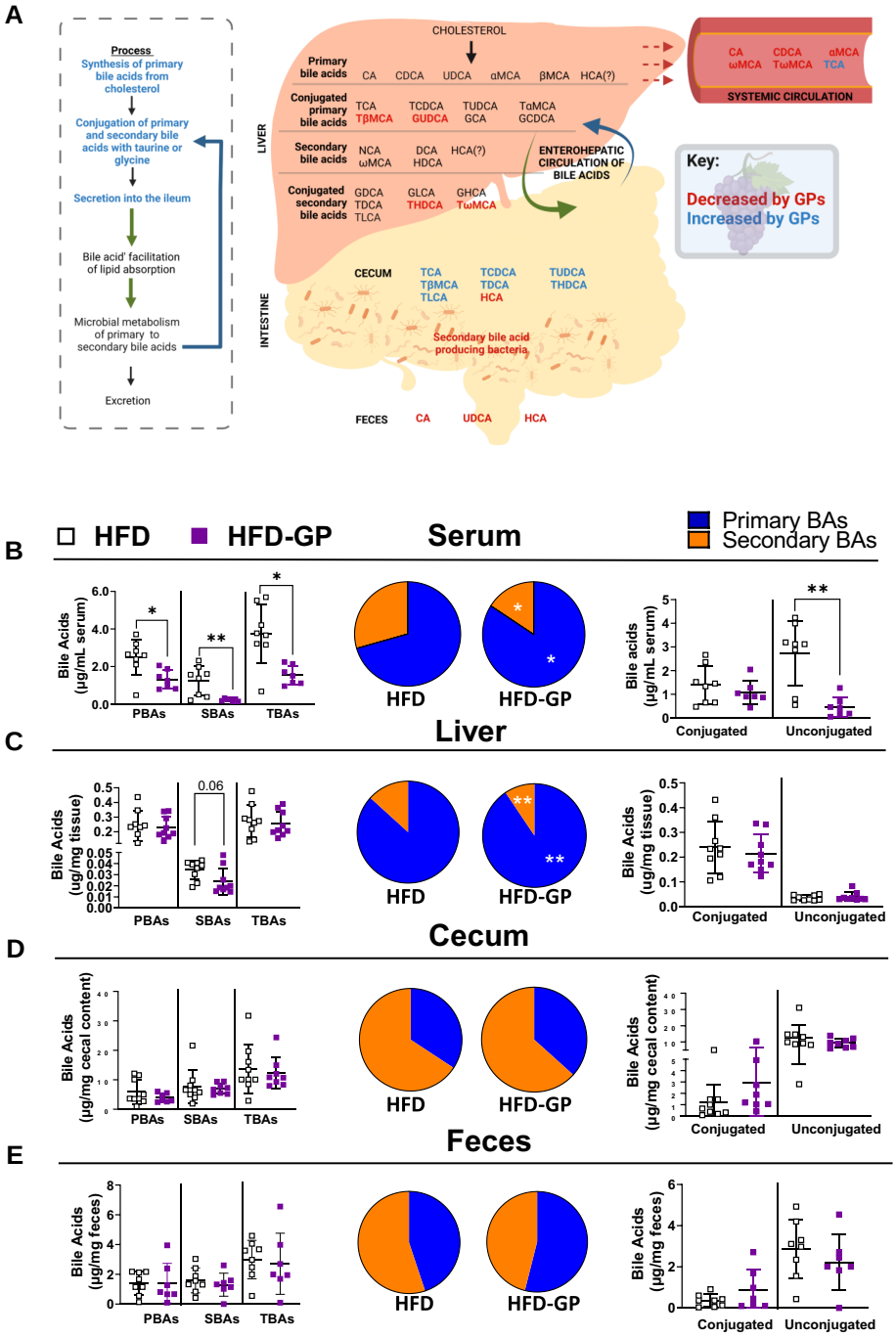

Figure 5. (A) Schematic summarizing changes to BA species across serum, liver, cecal, and feces induced by GPs. PBA are synthesized from cholesterol in the liver after which they may be conjugated with taurine (T) or glycine (G). BAs are secreted postprandially into the intestinal lumen to facilitate lipid absorption. Ninety-five percent of BAs are reabsorbed in the proximal intestine, but some BA that reach the distal intestine can be metabolized by bacteria to SBAs, which may be absorbed and conjugated, or excreted with feces. PBAs measured included CA, CDCA, UDCA, αMCA, βMCA, GHCA, GUDCA, TUDCA, GCDCA, TCDCA, TαMCA, TβMCA, GCA, TCA. SBAs measured included NCA, DCA, ωMCA, HDCA, THDCA, GDCA, TDCA, TωMCA, GLCA, TLCA. HCA has been described as both a PBA and SBA in mice; we have included HCA in the SBA pool. Graphic was created with Biorender.com. (B-E) Sum of PBA, SBA, and total bile acids (TBAs) (left panel) with pie chart displaying fraction of TBAs that are secondary vs primary in mice on corresponding diets (middle panel), and the sum of conjugated vs unconjugated bile acids in cardiac serum, liver tissue, cecal content from week 17, and fecal samples collected at week 15 (n = 7-9/group) (right panel). All values are presented as individual mouse value ± SD. Each symbol in scatter plots represents a single animal. Unpaired student t-tests of Mann–Whitney tests, for nonparametric data, was performed. *$P < .05$, **$P < .01$. Numerical P values are indicated when $.05 < P < .1$.

GP supplementation significantly reduced the relative abundance of phylum Firmicutes and increased Bacteroidetes and Verrucomicrobiota (Fig. 7D). The HFD-GP group had reduced Firmicutes-to-Bacteroidetes ratio (HFD: 9.11 vs HFD-GP: 5.1, $P = .001$), a general biomarker of a healthy gut community in mice [65]. Of the 127 taxa identified at the genus level, 13 taxa were significantly affected by GP supplementation. A group of Firmicutes genera were affected by GP supplementation, which led to reduction of *Allobaculum*, *Clostridium*, *Lactococcus*, *Ruminococcus*, *Syntrophomonas*, and *Turicibacter* but

Table 1. Bile acids quantified in serum, liver, cecal content, and feces

	Serum (μg/mL)		Liver (μg/mg)		Cecal content (μg/mg)		Feces (μg/mg)	
	HFD	HFD-GP	HFD	HFD-GP	HFD	HFD-GP	HFD	HFD-GP
Primary bile acids								
Unconjugated								
CA	0.81 ± 0.5	0.18 ± 0.14**	0.02 ± 0.007	0.02 ± 0.007	1 ± 1	0.6 ± 0.9	0.42 ± 0.36	0.07 ± 0.07*
CDCA	0.003 ± 0.002	0*	0.001 ± 0.0003	0.001 ± 0.0003	0.03 ± 0.03	0.02 ± 0.004	0.01 ± 0.005	0.008 ± 0.01
αMCA	0.008 ± 0.01	0.001 ± 0.003*	0.003 ± 0.001	0.004 ± 0.001	2.2 ± 1.6	1.4 ± 0.6	0.29 ± 0.23	0.19 ± 0.13
βMCA	0.55 ± 0.52	0.19 ± 0.33	0.02 ± 0.005	0.02 ± 0.01	0.8 ± 0.7	0.5 ± 0.2	0.4 ± 0.22	0.28 ± 0.15
UDCA	0	0	0.001 ± 0.0005	0.001 ± 0.0005	0.06 ± 0.05	0.03 ± 0.01	0.02 ± 0.009	0.01 ± 0.005*
Conjugated								
TCA	0.002 ± 0.003	0.62 ± 0.42***	0.15 ± 0.08	0.15 ± 0.06	0.13 ± 0.19	0.63 ± 0.79*	0.005 ± 0.009	0.001 ± 0.002
TCDCA	0	0	0.009 ± 0.004	0.008 ± 0.003	0.005 ± 0.009	0.05 ± 0.06**	0.003 ± 0.004	0.021 ± 0.028
TUDCA	0	0	0.0008 ± 0.001	0.001 ± 0.003	0.15 ± 0.3	1 ± 1.5**	0.0006 ± 0.003	0.002 ± 0.02
TαMCA	0.09 ± 0.06	0.07 ± 0.04	0.02 ± 0.008	0.02 ± 0.007	0.16 ± 0.25	0.23 ± 0.23	0.14 ± 0.12	0.54 ± 0.78
TβMCA	0.11 ± 0.08	0.05 ± 0.01	0.03 ± 0.01	0.01 ± 0.005*	0.17 ± 0.2	0.4 ± 0.3 *	0.12 ± 0.17	0.06 ± 0.03
GCA	0	0	0.001 ± 0.0004	0.001 ± 0.0005	0.001 ± 0.002	0.005 ± 0.01	0.001 ± 0.002	0.001 ± 0.002
GCDCA	0	0	0	0	0.002 ± 0.0009	0.002 ± 0.0004	0.004 ± 0.003	0.003 ± 0.002
GUDCA	0.2 ± 0.015	0.21 ± 0.04	$3.7 \times 10^{-5} \pm 9.3 \times 10^{-6}$	$2.9 \times 10^{-5} \pm 6.1 \times 10^{-6}$*	0.001 ± 0.001	0.0006 ± 0.0003	0.0005 ± 0.0005	0.0003 ± 0.0003
Secondary bile acids								
Unconjugated								
NCA	NM	NM	0.007 ± 0.006	0.009 ± 0.009	0.07 ± 0.06	0.06 ± 0.06	0.18 ± 0.13	0.24 ± 0.24
HCA	0	0	$7.20 \times 10^{-5} \pm 8.6 \times 10^{-5}$	0.0001 ± 0.0001	1.05 ± 0.7	0.35 ± 0.17**	0.36 ± 0.19	0.17 ± 0.09*
DCA	0.02 ± 0.03	0.03 ± 0.03	$0.0002 \pm 6.5 \times 10^{-005}$	0.0002 ± 0.0001	2.4 ± 0.97	3.3 ± 1.3	0.13 ± 0.11	0.13 ± 0.08
ωMCA	0.85 ± 0.74	0.001 ± 0.002***	0.003 ± 0.0007	0.003 ± 0.002	4.6 ± 5.5	2.9 ± 1.2	0.54 ± 0.38	0.45 ± 0.26
HDCA	0.12 ± 0.03	0.08 ± 0.07	0.0006 ± 0.0002	0.0008 ± 0.0005	0.25 ± 0.14	0.24 ± 0.08	0.11 ± 0.05	0.14 ± 0.09
Conjugated								
GHCA	0	0	0	0	0	0	0	0
GDCA	NM	NM	$2.4 \times 10^{-006} \pm 3.8 \times 10^{-012}$	$2.2 \times 10^{-012} \pm 3.6 \times 10^{-013}$	0.001 ± 0.0008	0.001 ± 0.0007	0.0004 ± 0.0003	0.0005 ± 0.0003
GLCA	0	0	$8.3 \times 10^{-006} \pm 1.2 \times 10^{-005}$	$1.7 \times 10^{-005} \pm 2.2 \times 10^{-005}$	0	0	0	0
TDCA	0.003 ± 0.001	0.002 ± 0.002	0.002 ± 0.0008	0.003 ± 0.002	0.04 ± 0.06	0.08 ± 0.07*	0.01 ± 0.01	0.03 ± 0.03
THDCA	0	0	0.003 ± 0.001	0.002 ± 0.0004*	0.02 ± 0.03	0.06 ± 0.06*	$3 \times 10^{-26} \pm 2.73 \times 10^{-005}$	0.0001 ± 0.0001
TLCA	NM	NM	$4.6 \times 10^{-6} \pm 9.2 \times 10^{-6}$	$1.5 \times 10^{-5} \pm 3 \times 10^{-5}$	0.001 ± 0.001	0.003 ± 0.002**	0.001 ± 0.003	0.005 ± 0.008
TωMCA	0.25 ± 0.13	0.11 ± 0.03*	0.03 ± 0.008	0.015 ± 0.009*	0.4 ± 0.5	0.5 ± 0.4	0.07 ± 0.06	0.14 ± 0.17

Values are presented as mean ± SD (n = 7-9/group). Normality was tested using Shapiro–Wilk test and group means were compared by unpaired t test for normally distributed data or Mann–Whitney test if nonparametric.

Abbreviations: αMCA, alpha-muricholic acid; βMCA, beta-muricholic acid; ωMCA, omega-muricholic acid; CA, cholic acid; CDCA, chenodeoxycholic acid; DCA, deoxycholic acid; GCA, glycocholic acid; GCDCA, glycochenodeoxycholic acid; GDCA, glycodeoxycholic acid; GHCA, glycohyocholic acid; GLCA, glycolithocholic acid; GP, grape polyphenol; GUDCA, glycoursodeoxycholic acid; HCA, hyocholic acid; HDCA, hyodeoxycholic acid; HFD, high-fat diet; NCA, nutracholic acid; NM, not measured; TαMCA, tauro-alpha-muricholic acid; TβMCA, tauro-beta-muricholic acid; TωMCA, tauro-omega-muricholic acid; TCA, taurocholic acid; TCDCA, taurochenodeoxycholic acid; TDCA, taurodeoxycholic acid; THDCA, taurohyodeoxycholic acid; TLCA, taurolithocholic acid; TUDCA, tauroursodeoxycholic acid; UDCA, ursodeoxycholic acid.

*$P < .05$; **$P < .001$.

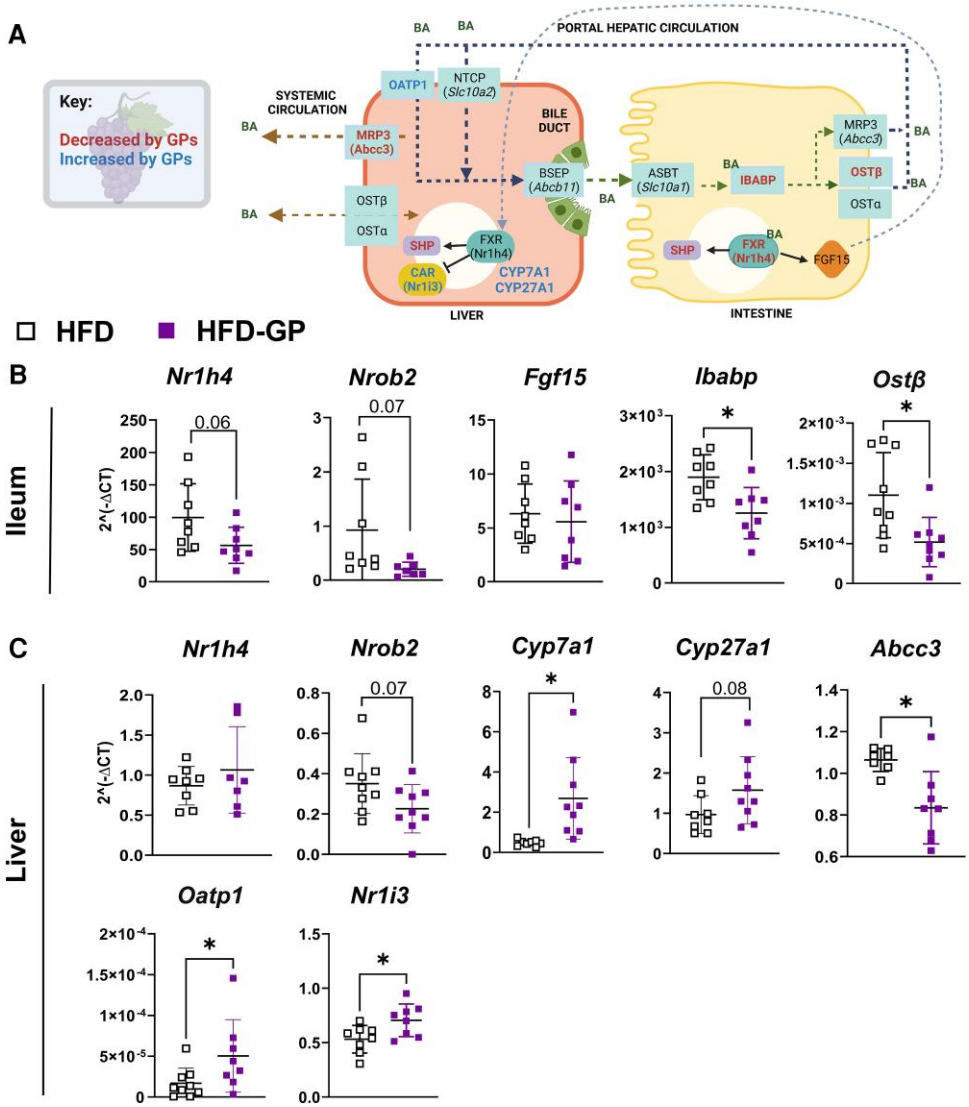

Figure 6. Markers of bile acid homeostasis. (A) Schematic displaying effects of GPs on FXR gene targets for BA regulation in hepatocyte and enterocyte cells. Typically, FXR activation in mice results in (1) downregulation of ileal apical sodium dependent BA transporter (ASBT; encoded by *Slc10a2*) to reduce intestinal BA reuptake, (2) increased intracellular ileal BA binding protein (IBABP) to promote transfer of BAs out of enterocytes, (3) increased hepatic and intestinal multidrug-resistant protein-3 (MRP3, encoded by *Abcc3*) and basolateral bidirectional transporters organic solute transporters (Ostα, Ostβ) to increase BA elimination from both hepatocytes and enterocytes, (4) increased hepatic bile salt export pump (BSEP; encoded by *Abcb11*) to promote BA secretion from hepatocytes, (5) decreased hepatic Na^+-taurocholate cotransporting polypeptide (NTCP encoded by *Slc10a1*) and organic anion-transporting polypeptides (OATp) to reduce BA flow into hepatocytes, and (6) decreased transactivation of BA synthesis enzymes (CYP7A1 and CYP27A1) [58, 59, 106]. Graphic was created with Biorender.com. (B) Ileal gene expression of farnesoid X receptor (FXR; encoded by *Nr1h4*), small heterodimer partner (SHP; *Nrob2*), fibroblast growth factor 15 (*Fgf15*), intestinal bile acid–binding protein (*Ibabp*), organic solute transporter beta (*Ostβ*). (C) Liver gene expression of *Nr1h4*, *Shp*, cholesterol 7 alpha-hydroxylase (*Cyp7a1*), cholesterol 27 alpha-hydroxylase (*Cyp27a1*), multidrug-resistant protein-3 (MRP3; *Abcc3*), organic anion-transporting peptides (*Oatp1*), constitutive androstane receptor (CAR; *Nr1i3*). n = 8-9/group; All values are presented as individual mouse value ± SD. Each symbol in scatter plots represents a single animal. Unpaired Student t tests of Mann–Whitney tests, for nonparametric data, was performed. *$P < .05$, Numerical P values are indicated when $.05 < P < .1$.

increased *Aldercreutzia*, *Dehalobacterium*, and *rc4-4* (Fig. 7E; Fig. 9A [34]). Several isolated genera within other phyla were altered by GPs, including a reduction to Spirochaetes genus *W22*, and increase to Proteobacteria genus *Suterella*, Bacteriodetes genus *Bacteroides*, and Verrucomicrobiota genus *Akkermansia* (Fig. 7E; Fig. 9B-E [34]). A GP-induced increase in *A. muciniphila* was confirmed by qPCR on fecal samples at week 3 and on cecal samples at week 17 of the diet intervention (Fig. 7F and 7G). Total bacterial load, as determined by qPCR, was not affected in fecal samples after 3 weeks of GP supplementation (Fig. 7H) but was significantly increased in cecal content at week 17 (Fig. 7I), revealing that supplementation of HFD with 0.5% GPs did not have a general antibacterial effect on the gut community.

Bacterial Genera Changed by GP Supplementation Correlated With Changed BA

To identify the relationship between the gut bacteria and BAs, Spearman's correlation analysis was performed between significantly changed genera and BAs in cecal content of both HFD and HFD-GP groups. Cecal levels of *Turicibacter*, *Allobaculum*, *Clostridium*, and *Syntrophomonas*, were negatively correlated with cecal levels of taurine conjugated BAs (ie, TUDCA, TCDCA, TβMCA, TCA, or TLCA) (Fig. 10

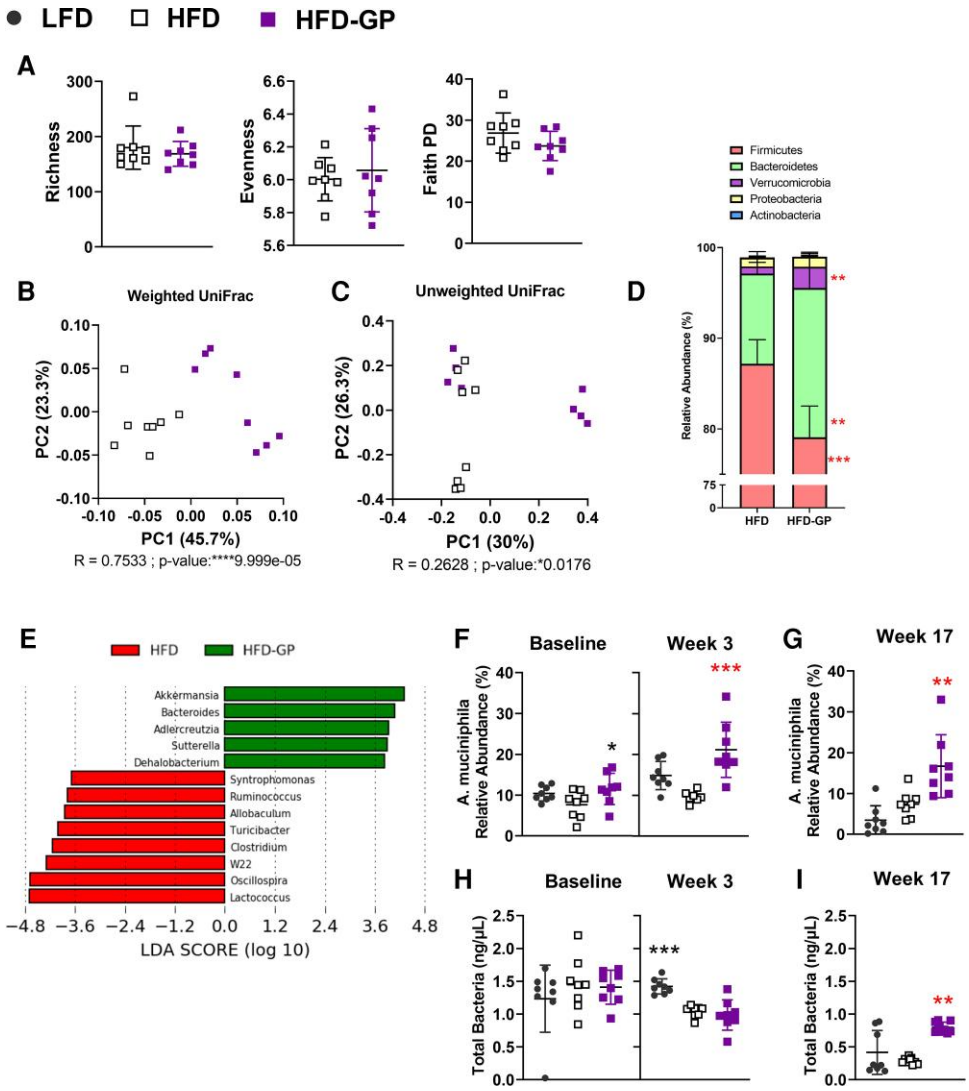

Figure 7. Effects of GPs on the cecal gut microbiota on a HFD. (A) α-Diversity metrics (ie, richness, evenness, and faith phylogenetic diversity [PD]). β-Diversity metrics (ie, weighted Unifrac and (C) unweighted Unifrac) analyzed by Adonis statistics. (D) Relative abundance of bacterial phyla. (E) Linear discriminant analysis effect size of taxa at the lowest taxonomic level possible that better discriminates the cecal gut microbiota of HFD verses HFD-GP-fed mice. *A. muciniphila* abundance in (F) feces at baseline (week 0) and week 3 and in (G) cecal content at week 17. (H) Total bacterial load in feces at baseline and week 3 and in (I) cecal content at week 17. n = 8/group. All values are presented as individual mouse value ± SD. Each symbol in scatter plots represents a single animal. Unpaired Student t tests or Mann–Whitney tests, for nonparametric data, was performed when 2 diet groups were analyzed. One-way ANOVA followed by Dunn's multiple comparison for parametric or Kruskal–Wallis followed by Dunnett's for nonparametric test was performed to compare 3 diet groups. Black asterisks indicate statistically significant values between HFD and LFD-fed mice, and red asterisks indicate statistically significant values between HFD and HFD-GP–fed mice. $^{*}P < .05$, $^{**}P < .01$, $^{***}P < .001$, $^{****}P < .0001$.

[34]); therefore, these taxa may metabolize these BA. Bacteria may convert HCA to HDCA [66]. *Akkermansia* negatively correlated with HCA (Fig. 10 [34]), revealing that *Akkermansia* may metabolize this BA.

Discussion

Polyphenols (eg, proanthocyanidins, anthocyanins, theaflavins, epigallocatechin gallate, hydroxycinnamates, or resveratrol) increased energy expenditure in obese mice or adults with obesity, suggesting a common mechanism by which polyphenols may reduce weight gain [5, 8, 67-71]. In our study, we show for the first time that GP supplementation elevated energy expenditure, reduced inflammation, liver fat, and BA accumulation, and changed the gut bacterial community in association with increased markers of HPAA activity (Fig. 8).

In leptin-receptor–deficient mice on a LFD, GP supplementation improved glucose metabolism, but did not reduce body weight gain or BA load [9]. Moreover, GP increased liver fat and markers of inflammation (ie, *Il1b*) in *db/db* leptin receptor–deficient mice (Fig. 11A-C [34]). Enzymes regulating CORT and BAs (ie, *Akr1d1*, *Srd5a1*, and *Nr1i3*) were not affected by GP supplementation in leptin-receptor deficient mice (Fig. 11D [34]). Downregulation of 11β-HSD1 and upregulation of AKR1D1 has been associated with reduced hepatic steatosis and metabolic syndrome [72-75]; therefore, changes to gene expression for these enzymes in GP-supplemented wild-type mice may be leptin dependent and important for metabolic improvements. Comparisons of the effects of GPs in wild-type to leptin receptor–deficient mice suggests that GP-induced improvements to glucose metabolism may be independent of leptin signaling, but leptin may play a key role

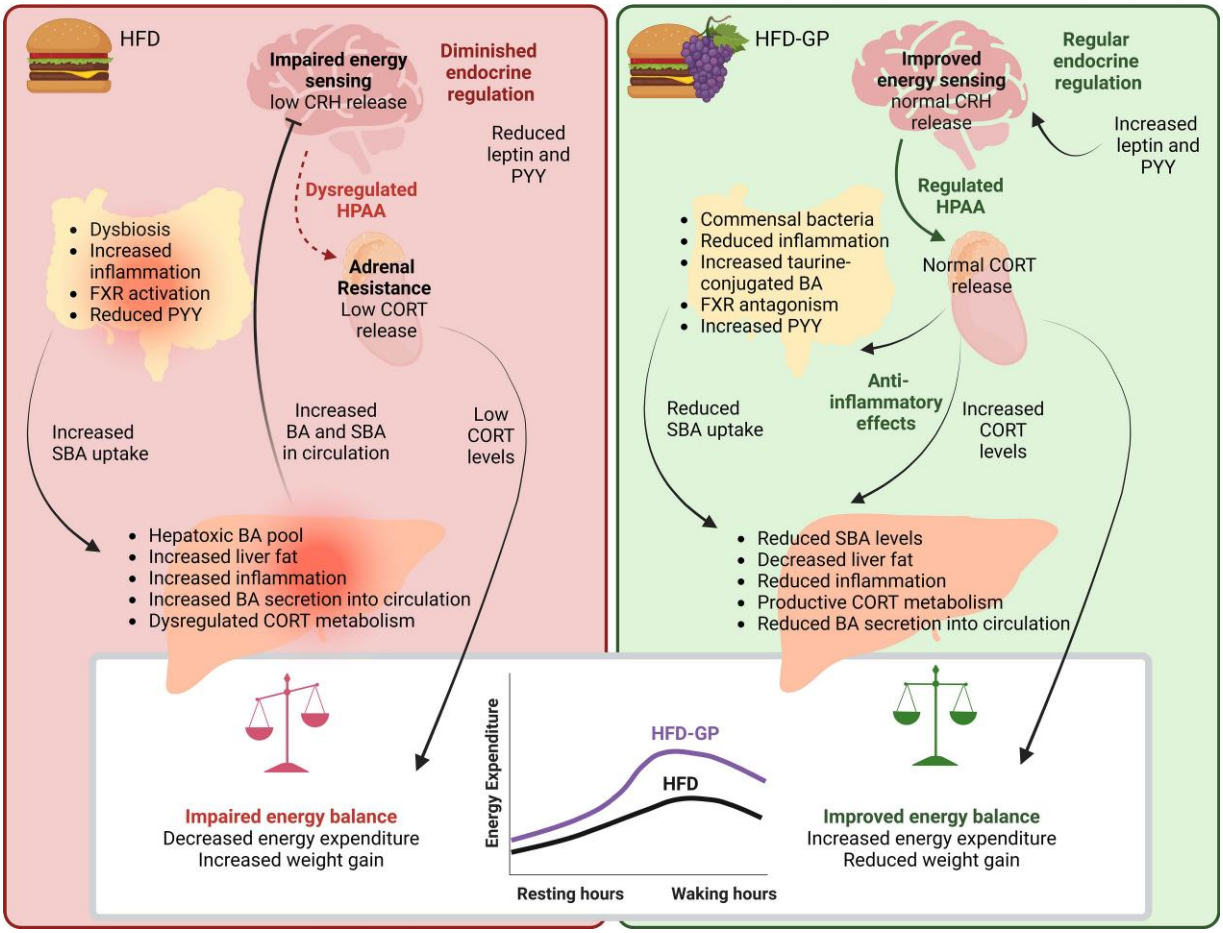

Figure 8. Potential mechanisms for the effects of GPs on HPAA control of energy balance, involving the gut bacteria, BA, and endocrine hormones.

in reducing BA load, protecting the liver, maintaining energy balance, and regulating CORT levels. Other studies have also noted a leptin effect, showing increased hypothalamic sensitivity to leptin [76] and preserved leptin levels with circadian rhythms to BA levels and genes in polyphenol supplemented rodents [77].

The low bioavailability of proanthocyanidins suggests that their metabolic improvements may begin in the gut lumen [78]. Polyphenol supplementation significantly alters the gut microbial community [4, 5, 9, 67, 79, 80], potentially leading to metabolic improvements through multiple mechanisms. GPs may prevent gut dysbiosis by acting as both an antibiotic to pathogenic bacteria and probiotic to commensal bacteria. The increase in *A. muciniphila* preceded metabolic improvements [6], indicating a potential causal role. *A. muciniphila* supplementation for elevated energy expenditure [81]. Various dietary polyphenols have been reported to increase *A. muciniphila* [4-6, 9, 67, 77, 82-87].

Reduced Firmicutes genera expressing 7α-dehydroxylase [88] (ie, *Clostridium*, *Lactococcus*, and *Ruminococcus* (Fig. 7E)) likely resulted in decreased SBA in GP-supplemented mice (Fig. 5B and 5C) which potentially reduced the cytotoxicity of the BA pool [28, 89]. Reductions to Firmicutes containing the deconjugating enzyme, bile salt hydrolase [90], can explain increased levels of taurine-conjugated BAs in cecal content of GP-supplemented mice. Conjugated BA species likely stay within the lumen for longer periods due to reduced permeability and reabsorption [91]; therefore, increased taurine-conjugated BAs could lead to increased BA signaling within the gut. Several taurine-conjugated species (ie, TLCA, TDCA, and TCA) have been reported to increase levels of PYY or leptin [92, 93], a correlation observed in GP supplemented mice (Figs. 3G and 5A). GP supplementation may reduce inflammation and HPAA-impairment by decreasing levels of hydrophobic and cytotoxic BA (ie, CA and CDCA; Fig. 5A) that compete with CORT clearing enzyme, AKR1D1 [12, 91]. Increased TCA and TDCA in the gut of GP supplemented mice suggests increased taurine-conjugation of CA and CDCA, and can explain their reduced levels in circulation (Fig. 5A). GPs may also indirectly change gut bacteria by altering the BA profile [88, 94]. For instance, studies have reported that CA increased *Clostridium* spp. [88], and TCA decreased *Turicibacter* abundance [94]—both correlations observed in GP-supplemented mice (Fig. 10 [34]).

Inhibition of FXR is being investigated as a potential treatment for cholestasis and glucose intolerance [95, 96]. GP supplementation in leptin receptor–deficient mice resulted in decreased abundance of SBA-producing bacteria shown to be FXR agonists, supported by reduced gene markers of intestinal FXR activation [9]. In this study, gene expression data suggested GPs redirected BA flow away from circulation by reducing FXR activity (Fig. 6A). Reduced FXR activity could be due to decreased levels of circulating FXR agonists, ωMCA, and TωMCA [9], and increased cecal levels of FXR antagonist, TβMCA [97] (Fig. 5A). The GP-induced reduction in circulating BA levels may have prevented BA-mediated

inhibition of the HPAA that is observed in rodents with high levels of circulating BA [12, 29-31]. Overall, GP supplementation appears to promote a less inflammatory and inhibitory BA profile in relation to the HPAA.

The impact of increased CORT levels in response to HFD is still under debate. While some report CORT as a marker of stress and metabolic disruption [98], others describe CORT production as a normal adaptation to increased metabolic demands [22]. Furthermore, studies report both increases and decreases to CORT in response to HFD [99]. Increased cortisol levels were detected in human subjects with obesity [100], but this may be an adaptation to weight gain rather than a causal factor. Our study suggests increased circulating and hepatic CORT are markers of improved HPAA function in mice with prolonged HFD intake. To investigate the effects of dietary polyphenols and develop pharmacological targets, a better understanding of the regulation of the HPAA is crucial.

The results of our study are correlative but provide novel insight to the role the HPAA may have behind GP-mediated metabolic resilience. To further investigate the effects of dietary polyphenols on the HPAA, future studies should be strictly time controlled, as numerous metabolites and genes follow circadian rhythms [77, 101]. Methods which can detect CORT and tetrahydrometabolite levels at different timepoints without inducing stress, such as via urine or feces [102], should be used. Furthermore, time of administration of polyphenols is an important variable affecting bioactivity [103], and thus controlled feeding is optimal to monitor effects on circadian phenotypes. Intervention studies should also explore effects of known sexual dimorphisms in CORT and leptin levels [104, 105]. Such studies are needed to elucidate if polyphenols promote health via effects on the HPAA.

Acknowledgments

Thank you to Rifke Anolik, Riya Patel, Sriya Sadangi, and Zehra Jaffri for their technical support, Rutgers Bartlett animal facility staff for their assistance with animal care, Alexander Poulev for LC-MS analysis of polyphenols, Deeptha Kumaraswamy of the IFNH GC-MS core facility for SCFA analysis, Marianne Polunas from Rutgers Research Pathology Services for slide preparation, to Research Diets for assistance with diet formulation, and Azenta Life Sciences (Piscataway, NJ) for sequencing services.

Funding

This work was supported by a Robert T. Rosen Memorial scholarship to EM, a Ruth L. Kirschstein NRSA Predoctoral Fellowship from National Institutes of Health, National Center for Complementary and Integrative Health (F31 AT010981) to KMT, and NIH-NCCIH Grant R01 AT010242 to DER.

Author Contributions

Conceptualization, E.M.; methodology, E.M., K.M.T., J.A.V., N.T.B., N.D., Y.W.; validation, E.M. and K.M.T.; formal analysis, E.M., K.M.T, J.A.V., N.D., D.K., A.C., Y.W., K.B.; investigation, E.M., K.M.T, J.A.V., N.D., D.K., A.C., Y.W., K.B., K.S.; resources, D.E.R., N.T.B.; data curation, E.M., K.M.T.; writing—original draft preparation, E.M.; writing—final review and editing, D.E.R.; visualization, E.M. K.M.T.; supervision, D.E.R., N.T.B.; project administration, D.E.R.; funding acquisition, D.E.R., K.M.T., E.M. All authors have read and agreed to the published version of the manuscript.

Disclosures

D.E.R. has equity in Nutrasorb LLC. The funders had no role in the design of the study; in the collection, analyses, or interpretation of data; in the writing of the manuscript, or in the decision to publish the results. The remaining authors declare that the research was conducted in the absence of any commercial or financial relationships that could be construed as a potential conflict of interest.

Data Availability

Original data generated and analyzed during this study are included in this published article or in the data repositories listed in References [34].

Data Transparency Statement

16S rRNA V3-V4 amplicon sequence files are available on sequence read archive under PRJNA890264.

Ethics Statement

The animal study was reviewed and approved by Rutgers institutional animal care and use committee.

References

1. Stinson EJ, Piaggi P, Ibrahim M, Venti C, Krakoff J, Votruba SB. High fat and sugar consumption during ad libitum intake predicts weight gain. *Obesity*. 2018;26(4):689-695.
2. Borgeraas H, Barstad LH, Størdal Lund R, Fredheim JM, Hertel JK, Hjelmesaeth J. Association of time of obesity onset with comorbidities in treatment-seeking men and women with severe obesity. *Obes Sci Pract*. 2018;4(5):427-436.
3. Roopchand DE, Kuhn P, Krueger CG, Moskal K, Lila MA, Raskin I. Concord grape pomace polyphenols complexed to soy protein isolate are stable and hypoglycemic in diabetic mice. *J Agric Food Chem*. 2013;61(47):11428-11433.
4. Roopchand DE, Carmody RN, Kuhn P, *et al*. Dietary polyphenols promote growth of the gut bacterium *Akkermansia muciniphila* and attenuate high-fat diet—induced metabolic syndrome. *Diabetes*. 2015;64(8):2847-2858.
5. Mezhibovsky E, Knowles KA, He Q, *et al*. Grape polyphenols attenuate diet-induced obesity and hepatic steatosis in mice in association with reduced butyrate and increased markers of intestinal carbohydrate oxidation. *Front Nutr*. 2021;8:675267.
6. Zhang L, Carmody RN, Kalariya HM, *et al*. Grape proanthocyanidin-induced intestinal bloom of *Akkermansia muciniphila* is dependent on its baseline abundance and precedes activation of host genes related to metabolic health. *J Nutr Biochem*. 2018;56:142-151.
7. Ginés I, Gil-Cardoso K, Terra X, *et al*. Grape seed proanthocyanidins target the enteroendocrine system in cafeteria-diet-fed rats. *Mol Nutr Food Res*. 2019;63(11):1800912.
8. Serrano J, Casanova-Martí À, Gual A, *et al*. A specific dose of grape seed-derived proanthocyanidins to inhibit body weight gain limits food intake and increases energy expenditure in rats. *Eur J Nutr*. 2017;56(4):1629-1636.
9. Tveter KM, Villa JA, Cabales AJ, *et al*. Polyphenol-induced improvements in glucose metabolism are associated with bile acid signaling to intestinal farnesoid X receptor. *BMJ Open Diabetes Res Care*. 2020;8(1):e001386.

10. Shin AC, MohanKumar SMJ, Balasubramanian P, *et al.* Responsiveness of hypothalamo–pituitary–adrenal axis to leptin is impaired in diet-induced obese rats. *Nutr Diabetes*. 2019; 9(1):10.
11. Toru Inoue AI, Okita M, Sakatani N, *et al.* Effect of neuropeptide Y on the hypothalamic–pituitary–adrenal axis in the dog. *Life Sci*. 1989;44(15):1043-1051.
12. McNeilly AD, Macfarlane DP, O'Flaherty E, *et al.* Bile acids modulate glucocorticoid metabolism and the hypothalamic–pituitary–adrenal axis in obstructive jaundice. *J Hepatol*. 2010;52(5): 705-711.
13. Herman JP, McKlveen JM, Ghosal S, *et al.* Regulation of the hypothalamic–pituitary–adrenocortical stress response. *Compr Physiol*. 2011;6(2):603-621.
14. Boersma GJ, Tamashiro KL, Moran TH, Liang NC. Corticosterone administration in drinking water decreases high-fat diet intake but not preference in male rats. *Am J Physiol Regul Integr Comp Physiol*. 2016;310(8):R733-R743.
15. Spiga F, Walker JJ, Terry JR, Lightman SL. HPA axis-rhythms. *Compr Physiol*. 2014;4(3):1273-1298.
16. Gong S, Miao YL, Jiao GZ, *et al.* Dynamics and correlation of serum cortisol and corticosterone under different physiological or stressful conditions in mice. *PLoS ONE*. 2015;10(2):e0117503.
17. Drake AJ, Livingstone DEW, Andrew R, Seckl JR, Morton NM, Walker BR. Reduced adipose glucocorticoid reactivation and increased hepatic glucocorticoid clearance as an early adaptation to high-fat feeding in Wistar rats. *Endocrinology*. 2005;146(2): 913-919.
18. Valanejad L, Nadolny C, Shiffka S, Chen Y, You S, Deng R. Differential feedback regulation of Δ4-3-oxosteroid 5β-reductase expression by bile acids. *PLoS ONE*. 2017;12(1):e0170960.
19. Nicolaides NC, Charmandari E, Chrousos GP, Kino T. Circadian endocrine rhythms: the hypothalamic–pituitary–adrenal axis and its actions. *Ann N Y Acad Sci*. 2014;1318(1):71-80.
20. Yang Y, Zhang J. Bile acid metabolism and circadian rhythms. *Am J Physiol Gastrointest Liver Physiol*. 2020;319(5):G549-G563.
21. Auvinen HE, Romijn JA, Biermasz NR, *et al.* The effects of high fat diet on the basal activity of the hypothalamus–pituitary–adrenal axis in mice. *J Endocrinol*. 2012;214(2):191-197.
22. Jimeno B, Hau M, Verhulst S. Corticosterone levels reflect variation in metabolic rate, independent of 'stress'. *Sci Rep*. 2018;8(1):13020.
23. Cooling J, Blundell J. Differences in energy expenditure and substrate oxidation between habitual high fat and low fat consumers (phenotypes). *Int J Obes*. 1998;22(7):612-618.
24. Cooling J, Barth J, Blundell J. The high-fat phenotype: is leptin involved in the adaptive response to a high fat (high energy) diet? *Int J Obes*. 1998;22(11):1132-1135.
25. Livingstone DE, Di Rollo EM, Yang C, *et al.* Relative adrenal insufficiency in mice deficient in 5alpha-reductase 1. *J Endocrinol*. 2014;222(2):257-266.
26. Navarrete J, Vásquez B, Vasconcellos A, Del Sol M, Olave E, Sandoval C. Effects of high-fat diets on biochemical profiles and morpho-quantitative characteristics of C57BL/6 mice adrenal glands. *Int J Morphol*. 2018;36(2):722-729.
27. Nianhong YA, Chongjian W, Mingjia X, Limei M, Liegang L, Xiufa S. Interaction of dietary composition and PYY gene expression in diet-induced obesity in rats. *J Huazhong Univ Sci Technolog Med Sci*. 2005;25(3):243-246.
28. Jena PK, Sheng L, Lucente JD, Jin L-W, Maezawa I, Wan Y-JY. Dysregulated bile acid synthesis and dysbiosis are implicated in Western diet—induced systemic inflammation, microglial activation, and reduced neuroplasticity. *FASEB J*. 2018;32(5): 2866-2877.
29. Quinn M, McMillin M, Galindo C, Frampton G, Pae HY, DeMorrow S. Bile acids permeabilize the blood brain barrier after bile duct ligation in rats via Rac1-dependent mechanisms. *Dig Liver Dis*. 2014;46(6):527-534.
30. McMillin M, Frampton G, Quinn M, *et al.* Suppression of the HPA axis during cholestasis can be attributed to hypothalamic bile acid signaling. *Mol Endocrinol*. 2015;29(12):1720-1730.
31. Petrescu AD, Kain J, Liere V, Heavener T, DeMorrow S. Hypothalamus–pituitary–adrenal dysfunction in cholestatic liver disease. *Front Endocrinol*. 2018;9:660.
32. Singleton VL, Rossi JA. Colorimetry of total phenolics with phosphomolybdic–phosphotungstic acid reagents. *Am Soc Enol Vitic*. 1965;16(3):144-158.
33. Sintara M, Li L, Cunningham DG, Prior RL, Wu X, Chang T. Single-laboratory validation for determination of total soluble proanthocyanidins in cranberry using 4-dimethylaminocinnamaldehyde. *J AOAC Int*. 2018;101(3):805-809.
34. Esther Mezhibovsky KMT, Villa-Rodriguez JA, Bacalia K, *et al.* Data from: supplementary materials for: grape polyphenols may prevent high fat diet-induced dampening of the hypothalamic–pituitary–adrenal axis in male mice. 2023. *Zenodo*. Deposited July 13, 2023. https://doi.org/10.5281/zenodo.8145865
35. Kamakura R, Kovalainen M, Leppaluoto J, Herzig KH, Makela KA. The effects of group and single housing and automated animal monitoring on urinary corticosterone levels in male C57BL/6 mice. *Physiol Rep*. 2016;4(3):e12703.
36. Liu X, Wu R, Tai F, *et al.* Effects of group housing on stress induced emotional and neuroendocrine alterations. *Brain Res*. 2013;1502:71-80.
37. Lusk G. *The Elements of the Science of Nutrition*. 2nd ed. W. B. Saunders & Co; 1909.
38. García-Villalba R, Giménez-Bastida JA, García-Conesa MT, Tomás-Barberán FA, Carlos Espín J, Larrosa M. Alternative method for gas chromatography-mass spectrometry analysis of short-chain fatty acids in faecal samples. *J Sep Sci*. 2012;35(15): 1906-1913.
39. Callahan BJ, McMurdie PJ, Rosen MJ, Han AW, Johnson AJA, Holmes SP. DADA2: high-resolution sample inference from Illumina amplicon data. *Nat Methods*. 2016;13(7):581-583.
40. Katoh K, Misawa K, Kuma KI, Miyata T. MAFFT: a novel method for rapid multiple sequence alignment based on fast Fourier transform. Comparative study. *Nucleic Acids Res*. 2002;30(14): 3059-3066.
41. Price MN, Dehal PS, Arkin AP. Fasttree 2—approximately maximum-likelihood trees for large alignments. *PLoS ONE*. 2010;5(3):e9490.
42. Faith DP. Conservation evaluation and phylogenetic diversity. *Biol Conserv*. 1992;61(1):1-10.
43. Lozupone C, Knight R. Unifrac: a new phylogenetic method for comparing microbial communities. *Appl Environ Microbiol*. 2005;71(12):8228-8235.
44. Bokulich NA, Kaehler BD, Rideout JR, *et al.* Optimizing taxonomic classification of marker-gene amplicon sequences with QIIME 2's q2-feature-classifier plugin. *Microbiome*. 2018;6(1): 1-17.
45. Guillod-Maximin E, Lorsignol A, Alquier T, Penicaud L. Acute intracarotid glucose injection towards the brain induces specific c-fos activation in hypothalamic nuclei: involvement of astrocytes in cerebral glucose-sensing in rats. *J Neuroendocrinol*. 2004;16(5):464-471.
46. Hills AP, Mokhtar N, Byrne NM. Assessment of physical activity and energy expenditure: an overview of objective measures. *Front Nutr*. 2014;1:5.
47. Zell V, Juif PE, Hanesch U, Poisbeau P, Anton F, Darbon P. Corticosterone analgesia is mediated by the spinal production of neuroactive metabolites that enhance GABAergic inhibitory transmission on dorsal horn rat neurons. *Eur J Neurosci*. 2015;41(3): 390-397.
48. Yoshihara S, Morimoto H, Ohori M, Yamada Y, Abe T, Arisaka O. A neuroactive steroid, allotetrahydrocorticosterone inhibits sensory nerves activation in guinea-pig airways. *Neurosci Res*. 2005;53(2):210-215.

49. Hideo Makimura TMM, Beasley J, Silverstein JH. Adrenalectomy stimulates hypothalamic proopiomelanocortin expression but does not correct diet-induced obesity. *BMC Physiol*. 2003;3:4.
50. George Mastorakos MGP, Mizamtsidi M. The hypothalamic–pituitary–adrenal and the hypothalamic–pituitary–gonadal axes interplay. *Pediatr Endocrinol Rev*. 2006;1(Suppl 1):172-181.
51. Zhang D, Tong X, VanDommelen K, *et al*. Lipogenic transcription factor ChREBP mediates fructose-induced metabolic adaptations to prevent hepatotoxicity. *J Clin Invest*. 2017;127(7):2855-2867.
52. Lin Z, Pan X, Wu F, *et al*. Fibroblast growth factor 21 prevents atherosclerosis by suppression of hepatic sterol regulatory element-binding protein-2 and induction of adiponectin in mice. *Circulation*. 2015;131(21):1861-1871.
53. Walker AK, Näär AM. SREBPs: regulators of cholesterol/lipids as therapeutic targets in metabolic disorders, cancers and viral diseases. *Clin Lipidol*. 2012;7(1):27-36.
54. Xu J, Lloyd DJ, Hale C, *et al*. Fibroblast growth factor 21 reverses hepatic steatosis, increases energy expenditure, and improves insulin sensitivity in diet-induced obese mice. *Diabetes*. 2009;58(1):250-259.
55. Fisher M, Chui PC, Antonellis PJ, *et al*. Obesity is a fibroblast growth factor 21 (FGF21)-resistant state. *Diabetes*. 2010;59(11):2781-2789.
56. Ahima RS. Revisiting leptin's role in obesity and weight loss. *J Clin Investig*. 2008;118(7):2380-2383.
57. Jagsi R, Jiang J, Momoh AO, *et al*. Metabolic adaptive ALT isoenzyme response in livers of C57/BL6 mice treated with dexamethasone. *Toxicol Pathol*. 2017;263(2):219-227.
58. Kim I, Ahn SH, Inagaki T, *et al*. Differential regulation of bile acid homeostasis by the farnesoid X receptor in liver and intestine. *J Lipid Res*. 2007;48(12):2664-2672.
59. Chiang JYL. Bile acids: regulation of synthesis. *J Lipid Res*. 2009;50(10):1955-1966.
60. Maeda T, Miyata M, Yotsumoto T, *et al*. Regulation of drug transporters by the farnesoid X receptor in mice. *Mol Pharmaceut*. 2004;1(4):281-289.
61. Beilke LD, Aleksunes LM, Holland RD, *et al*. Constitutive androstane receptor-mediated changes in bile acid composition contributes to hepatoprotection from lithocholic acid-induced liver injury in mice. *Drug Metab Dispos*. 2009;37(5):1035-1045.
62. Garcia M, Thirouard L, Sedes L, *et al*. Nuclear receptor metabolism of bile acids and xenobiotics: a coordinated detoxification system with impact on health and diseases. *Int J Mol Sci*. 2018;19(11):3630.
63. Everard A, Belzer C, Geurts L, *et al*. Cross-talk between *Akkermansia muciniphila* and intestinal epithelium controls diet-induced obesity. *Proc Natl Acad Sci USA*. 2013;110(22):9066-9071.
64. Mezhibovsky E, Wu Y, Bawagan FG, Tveter KM, Szeto S, Roopchand D. Impact of grape polyphenols on *Akkermansia muciniphila* and the gut barrier. *AIMS Microbiol*. 2022;8(4):544-565.
65. Magne F, Gotteland M, Gauthier L, *et al*. The Firmicutes/Bacteroidetes ratio: a relevant marker of gut dysbiosis in obese patients? *Nutrients*. 2020;12(5):1474.
66. Eyssen HJ, De Pauw G, Van Eldere J. Formation of hyodeoxycholic acid from muricholic acid and hyocholic acid by an unidentified gram-positive rod termed HDCA-1 isolated from rat intestinal microflora. *Appl Environ Microbiol*. 1999;65(7):3158-3163.
67. Anhê FF, Nachbar RT, Varin TV, *et al*. Treatment with camu camu (*Myrciaria dubia*) prevents obesity by altering the gut microbiota and increasing energy expenditure in diet-induced obese mice. *Gut*. 2019;68(3):453-464.
68. Kudo N, Arai Y, Suhara Y, Ishii T, Nakayama T, Osakabe N. A single oral administration of theaflavins increases energy expenditure and the expression of metabolic genes. *PLoS ONE*. 2015;10(9):e0137809.
69. Most J, Goossens GH, Jocken JW, Blaak EE. Short-term supplementation with a specific combination of dietary polyphenols increases energy expenditure and alters substrate metabolism in overweight subjects. *Int J Obes*. 2014;38(5):698-706.
70. Zhou J, Mao L, Xu P, Wang Y. Effects of (−)-epigallocatechin gallate (EGCG) on energy expenditure and microglia-mediated hypothalamic inflammation in mice fed a high-fat diet. *Nutrients*. 2018;10(11):1681.
71. Ibars M, Aragones G, Ardid-Ruiz A, *et al*. Seasonal consumption of polyphenol-rich fruits affects the hypothalamic leptin signaling system in a photoperiod-dependent mode. *Sci Rep*. 2018;8(1):13572.
72. Nikolaou N, Gathercole LL, Marchand L, *et al*. AKR1D1 Is a novel regulator of metabolic phenotype in human hepatocytes and is dysregulated in non-alcoholic fatty liver disease. *Metab Clin Exp*. 2019;99:67-80.
73. Li H, Sheng J, Wang J, *et al*. Selective inhibition of 11β-hydroxysteroid dehydrogenase type 1 attenuates high-fat diet-induced hepatic steatosis in mice. *Drug Des Dev Ther*. 2021;15:2309-2324.
74. Feig PU, Shah S, Hermanowski-Vosatka A, *et al*. Effects of an 11β-hydroxysteroid dehydrogenase type 1 inhibitor, MK-0916, in patients with type 2 diabetes mellitus and metabolic syndrome. *Diabetes Obes Metab*. 2011;13(6):498-504.
75. Drury JE, Mindnich R, Penning TM. Characterization of disease-related 5β-reductase (AKR1D1) mutations reveals their potential to cause bile acid deficiency. *J Biol Chem*. 2010;285(32):24529-24537.
76. Ibars M, Ardid-Ruiz A, Suárez M, Muguerza B, Bladé C, Aragonès G. Proanthocyanidins potentiate hypothalamic leptin/STAT3 signalling and Pomc gene expression in rats with diet-induced obesity. *Int J Obes*. 2017;41(1):129-136.
77. Cui Y, Yin Y, Li S, *et al*. Apple polyphenol extract modulates bile acid metabolism and gut microbiota by regulating the circadian rhythms in daytime-restricted high fat diet feeding C57BL/6 male mice. *Food Funct*. 2022;13(5):2805-2822.
78. Marin L, Miguelez EM, Villar CJ, Lombo F. Bioavailability of dietary polyphenols and gut microbiota metabolism: antimicrobial properties. *Biomed Res Int*. 2015;2015:905215.
79. Jang S, Sun J, Chen P, *et al*. Flavanol-enriched cocoa powder alters the intestinal microbiota, tissue and fluid metabolite profiles, and intestinal gene expression in pigs. *J Nutr*. 2016;146(4):673-680.
80. Wang J, Tang L, Zhou H, *et al*. Long-term treatment with green tea polyphenols modifies the gut microbiome of female Sprague–Dawley rats. *J Nutr Biochem*. 2018;56:55-64.
81. Depommier C, Van Hul M, Everard A, Delzenne NM, De Vos WM, Cani PD. Pasteurized *Akkermansia muciniphila* increases whole-body energy expenditure and fecal energy excretion in diet-induced obese mice. *Gut Microbes*. 2020;11(5):1231-1245.
82. Roopchand DE, Kuhn P, Rojo LE, Lila MA, Raskin I. Blueberry polyphenol-enriched soybean flour reduces hyperglycemia, body weight gain and serum cholesterol in mice. *Pharmacol Res*. 2013;68(1):59-67.
83. Anhê FF, Roy D, Pilon G, *et al*. A polyphenol-rich cranberry extract protects from diet-induced obesity, insulin resistance and intestinal inflammation in association with increased *Akkermansia* spp. Population in the gut microbiota of mice. *Gut*. 2015;64(6):872-883.
84. Ezzat-Zadeh Z, Henning SM, Yang J, *et al*. California Strawberry consumption increased the abundance of gut microorganisms related to lean body weight, health and longevity in healthy subjects. *Nutr Res*. 2021;85:60-70.
85. Sung MM, Kim TT, Denou E, *et al*. Improved glucose homeostasis in obese mice treated with resveratrol is associated with alterations in the gut microbiome. *Diabetes*. 2017;66(2):418-425.
86. Gao X, Xie Q, Kong P, *et al*. Polyphenol- and caffeine-rich postfermented Pu-erh tea improves dietinduced metabolic syndrome by remodeling intestinal homeostasis in mice. *Infect Immunity*. 2018;86(1):e00601-17.
87. Li Q, Liu F, Liu J, Liao S, Zou Y. Mulberry leaf polyphenols and fiber induce synergistic antiobesity and display a modulation effect on gut microbiota and metabolites. *Nutrients*. 2019;11(5):1017.

88. Ridlon JM, Alves JM, Hylemon PB, Bajaj JS. Cirrhosis, bile acids and gut microbiota: unraveling a complex relationship. *Gut Microbes*. 2013;4(5):382-387.
89. Lin H, An Y, Tang H, Wang Y. Alterations of bile acids and gut microbiota in obesity induced by high fat diet in rat model. *J Agric Food Chem*. 2019;67(13):3624-3632.
90. Geng W, Lin J. Bacterial bile salt hydrolase: an intestinal microbiome target for enhanced animal health. *Anim Health Res Rev*. 2016;17(2):148-158.
91. Hofmann AF. The continuing importance of bile acids in liver and intestinal disease. *Arch Intern Med*. 1999;159(22):2647-2658.
92. Christiansen CB, Trammell SAJ, Albrechtsen NJW, *et al.* Bile acids drive colonic secretion of glucagon-like-peptide 1 and peptide-YY in rodents. *Am J Physiol Gastrointest Liver Physiol*. 2019;316(5):G574-G584.
93. Levy JR, Heuman DM, Pandak WM, Stevens W. Effect of bile acid composition and manipulation of enterohepatic circulation on leptin gene regulation. *Metab Clin Exp*. 1998;47(3):285-291.
94. Kemis JH, Linke V, Barrett KL, *et al.* Genetic determinants of gut microbiota composition and bile acid profiles in mice. *PLoS Genet*. 2019;15(8):e1008073.
95. Stedman C, Liddle C, Coulter S, *et al.* Benefit of farnesoid X receptor inhibition in obstructive cholestasis. *Proc Natl Acad Sci USA*. 2006;103(30):11323-11328.
96. Jiang C, Xie C, Lv Y, *et al.* Intestine-selective farnesoid X receptor inhibition improves obesity-related metabolic dysfunction. *Nat Commun*. 2015;6(1):1-18.
97. Sayin SI, Wahlström A, Felin J, *et al.* Gut microbiota regulates bile acid metabolism by reducing the levels of tauro-beta-muricholic acid, a naturally occurring FXR antagonist. *Cell Metab*. 2013;17(2):225-235.
98. Tsai SF, Hung HC, Shih MM, *et al.* High-fat diet-induced increases in glucocorticoids contribute to the development of non-alcoholic fatty liver disease in mice. *FASEB J*. 2022;36(1):e22130.
99. Auvinen HE, Romijn JA, Biermasz NR, *et al.* Effects of high fat diet on the basal activity of the hypothalamus–pituitary–adrenal axis in mice: a systematic review. *Horm Metab Res*. 2011;43(13):899-906.
100. Andrew R, Phillips D, Brian W. Obesity and gender influence cortisol secretion and metabolism in man. *J Clin Endocrinol Metab*. 1998;83(5):1806-1809.
101. Soliz-Rueda JR, Lopez-Fernandez-Sobrino R, Bravo FI, Aragones G, Suarez M, Muguerza B. Grape seed proanthocyanidins mitigate the disturbances caused by an abrupt photoperiod change in healthy and obese rats. *Nutrients*. 2022;14(9):1834.
102. Bamberg E, Palme R, Meingassner JG. Excretion of corticosteroid metabolites in urine and faeces of rats. *Lab Anim*. 2001;35(4):307-314.
103. Ribas-Latre A, Del Bas JM, Baselga-Escudero L, *et al.* Dietary proanthocyanidins modulate melatonin levels in plasma and the expression pattern of clock genes in the hypothalamus of rats. *Mol Nutr Food Res*. 2015;59(5):865-878.
104. Seale JV, Wood SA, Atkinson HC, *et al.* Gonadectomy reverses the sexually diergic patterns of circadian and stress-induced hypothalamic–pituitary–adrenal axis activity in male and female rats. *J Neuroendocrinol*. 2004;16(6):516-524.
105. Priego T, Sanchez J, Palou A, Pico C. Effect of high-fat diet feeding on leptin receptor expression in white adipose tissue in rats: depot- and sex-related differential response. *Genes Nutr*. 2009;4(2):151-156.
106. Bryan Goodwin SAJ, Price RR, Michael A. Watson DDM, *et al.* A regulatory cascade of the nuclear receptors FXR, SHP-1, and LRH-1 represses bile acid biosynthesis. *Mol Cell*. 2000;6(3):517-526.